In situ-produced 10 Be and 26 Al indirect dating of Elarmékora Earlier Stone Age artifacts: first attempt in a savannah forest mosaic in the middle Ogooué valley, Gabon

Regis Braucher, Richard Oslisly, I Mesfin, P P Ntoutoume Mba, Team Aster

HAL Id: hal-03426405

https://amu.hal.science/hal-03426405

Submitted on 12 Nov 2021

In situ-produced [10]Be and [26]Al indirect dating of Elarmékora Earlier Stone Age artifacts: first attempt in a savannah forest mosaic in the middle Ogooué valley, Gabon.

R. Braucher[1,*], R. Oslisly[2, 3], I. Mesfin[4], P.P. Ntoutoume Mba[2] & ASTER Team[1,&]

1. Aix-Marseille Univ., CNRS-IRD-Collège de France-INRAE, UM 34 CEREGE, BP 80, 13545 Aix-en-Provence Cedex 4, France.
2. Cellule Scientifique, Agence Nationale des Parcs Nationaux, BP 20379 Libreville, Gabon.
3. Patrimoines Locaux Environnement et Globalisation UMR 208, IRD, MNHN, 57 rue Cuvier - C.P. 51, 75231 Paris cedex 05, France.
4. Muséum National d'Histoire Naturelle, UMR 7194 HNHP – MNHN, CNRS, UPVD – Alliance Sorbonne Université. Institut de Paléontologie Humaine, 1 rue René Panhard, 75013 Paris, France.

&. ASTER Team: Aumaître G., Bourlès D. and Keddadouche K.

*Author for correspondence (braucher@cerege.fr).

Abstract

Discovered in 1987 by R. Oslisly, Elarmékora is a high terrace that, today, is situated 175 m above the Ogooué River in the historical complex of Elarmékora, attached to the Lopé National Park in Gabon, a World Heritage site since 2007. The site yielded a small lithic assemblage, including mainly cobble artifacts embedded within the one-meter thick alluvial material. Based on geomorphological and palaeoclimatological criteria, the preliminary dating suggested an age of 400 ka. However, Elarmékora could be a key site for Atlantic Central Africa if this lithic industry can be dated absolutely.

In 2018 and 2019, two field trips were organized to collect surface samples as well as samples in vertical depth profiles with the aim of measuring their in-situ produced cosmogenic nuclide ([10]Be and [26]Al) content.

Results suggest a surface abandonment between 730 and 620 ka ago representing a minimum age for the cobble artifacts. Concurrently, technological reappraisal of the artifacts suggests an atypical lithic industry which should, for the moment, be considered as "undiagnostic" Earlier Stone Age. This age bracketing may be compared with a similar age range obtained for prehistoric occupations in Angola using the same approach. This age will place Elarmékora among the oldest evidence for the presence of hominins in western Central Africa and raises the question of a "West Side Story" to early human dispersals in Africa.

Introduction

In Africa, the major contribution of Earlier Stone Age archaeology in recent decades has been the establishment of a multidisciplinary approach combining palaeoenvironmental, palaeoanthropological and behavioral data within an increasingly reliable chronological framework. These data have allowed the

reconstruction of global trends in human evolution in Africa from the first stone-tool makers, 3.3 Ma ago [1] to the emergence of *Homo sapiens* ca. 300 ka ago [2]. This long period, namely the Earlier Stone Age (ESA), is divided into two main techno-complexes based on chronological and techno-typological criteria: the Oldowan and the Acheulean. The Oldowan is a flake and core industry sometimes associated with a pebble (4–64 mm) and cobble (64–256 mm) tool component [3,4], ranging from 2.58 Ma [5] to ca.1.5 Ma. So far it is only reported in eastern, southern and northern Africa [6]. The subsequent Acheulean techno-complex, broadly associated with the genus *Homo*, is considered as the first technology to be widespread over the entire African continent and beyond, especially since ca. 1 Ma [7–9]. However, once again, this techno-complex is best known from eastern, southern and northern African, with a large gap in our knowledge still for Central and West Africa. The Acheulean is characterized by the emergence and development of bifacial shaping, new flaking methods, large flake production (>10 cm) and specific new tool-types among which are Large Cutting Tools such as handaxes and cleavers [10–14]. Some Acheulean technical patterns are believed to have persisted until the Late Pleistocene in some regions [15]. There are very few dates and geoarchaeological studies available for ESA sites in Central Africa, an area which covers the Atlantic coast to the African Great Rift Lakes, spanning from Chad to Angola [16]. It also covers a broad range environmentally, characterized by Soudano-Zambezian environments in its periphery and Guineo-Congolian environments in its center [17].

However, a major limitation in current prehistoric research in Central Africa is its poorly-resolved Pleistocene chronological and techno-cultural framework [18]. The underlying reasons for this relate both to research bias, with little specific scientific research carried out, and taphonomy, with vegetation such as tropical forest or certain climatic conditions erasing or disturbing potential evidence of past human occupation [19–21]. Also, despite the fact that several sites have suggested the presence of hominin groups in the region during the ESA [22–27], only the site of Dungo IV in Angola, located at the southern limit of Central Africa, has been dated, with an age of ca. 600–650 ka [28]. However, this evidence is insufficient for assessing dispersal process(es) in the region, neither providing a robust palaeoenvironmental reconstruction for the specific equatorial environments of the time, nor defining the hominin technical and subsistence behaviors which prevailed in the equatorial belt of Central Africa. The site of Elarmékora in the middle valley of the Ogooué River in the Lopé National Park, central Gabon, possesses numerous alluvial deposits amalgamating ESA cobble artifacts [30]. While it was discovered at the end of the 1980s, renewed consideration of the site can challenge our current understanding of early Middle Pleistocene technological variability and population dispersal within sub-Saharan Africa.

Typologically ESA stone artifacts were found at Elarmékora in 1988 within an alluvial terrace perched 175 m above the Ogooué River (Fig. 2). As no source of quartz (like stone lines) can be found in the middle Ogooué valley, above an altitude of 250 m, the presence of the studied stone artefacts in these deposits is puzzling.

Figure 1: Stone artifacts from Elarmékora. A and B are core-tools presenting bidirectional flaking followed by unifacial regulating retouch sequence. C is a shaped tool on angular cobble. In [29], artifact A is illustrated as n°2, B as n°1 and C as n°13.

Site presentation

The studied site is located near the Otoumbi railway station (-0.09408 S; 11.17027 E; ~240 m above sea level and ~175 m above the Ogooué River) in the northwestern part of the World Heritage site "Ecosystem and Relict Cultural Landscape of Lopé-Okanda" (Fig2-A). In this region of central Gabon, dense and well-conserved tropical rainforest coexists with relict savannah environments. A 1.2 m high exposure of the alluvial terrace can be observed near an old path formerly used in logging activities.

The Elarmékora site was probably connected to an old erosion glacis where a paleo-Ogooué has left deposits overlying artifacts, subsequently flowing in a wider valley under arid climatic conditions which can be connected to the Middle Brunhes period [29]. Then, due to tectonic changes, the river started incising the relief, implying high denudation rates that have dismantled the old glacis and left the elevated deposits untouched. One can observe an alluvial deposit composed of rounded quartz cobbles (1–10 cm) embedded in a reddish sandy matrix and underlying a homogenous autochthonous saprolite. It is at the interface of the alluvial deposit and the saprolite (~90 cm under the surface) where [29] have described lithic artifacts. These

artifacts have thus been produced before their alluvial deposition at a higher elevation. Due to its dominant position and the smooth relief, one cannot observe any lateral displacements or potential arrival of colluvium from higher up that may have buried the original deposits at the site.
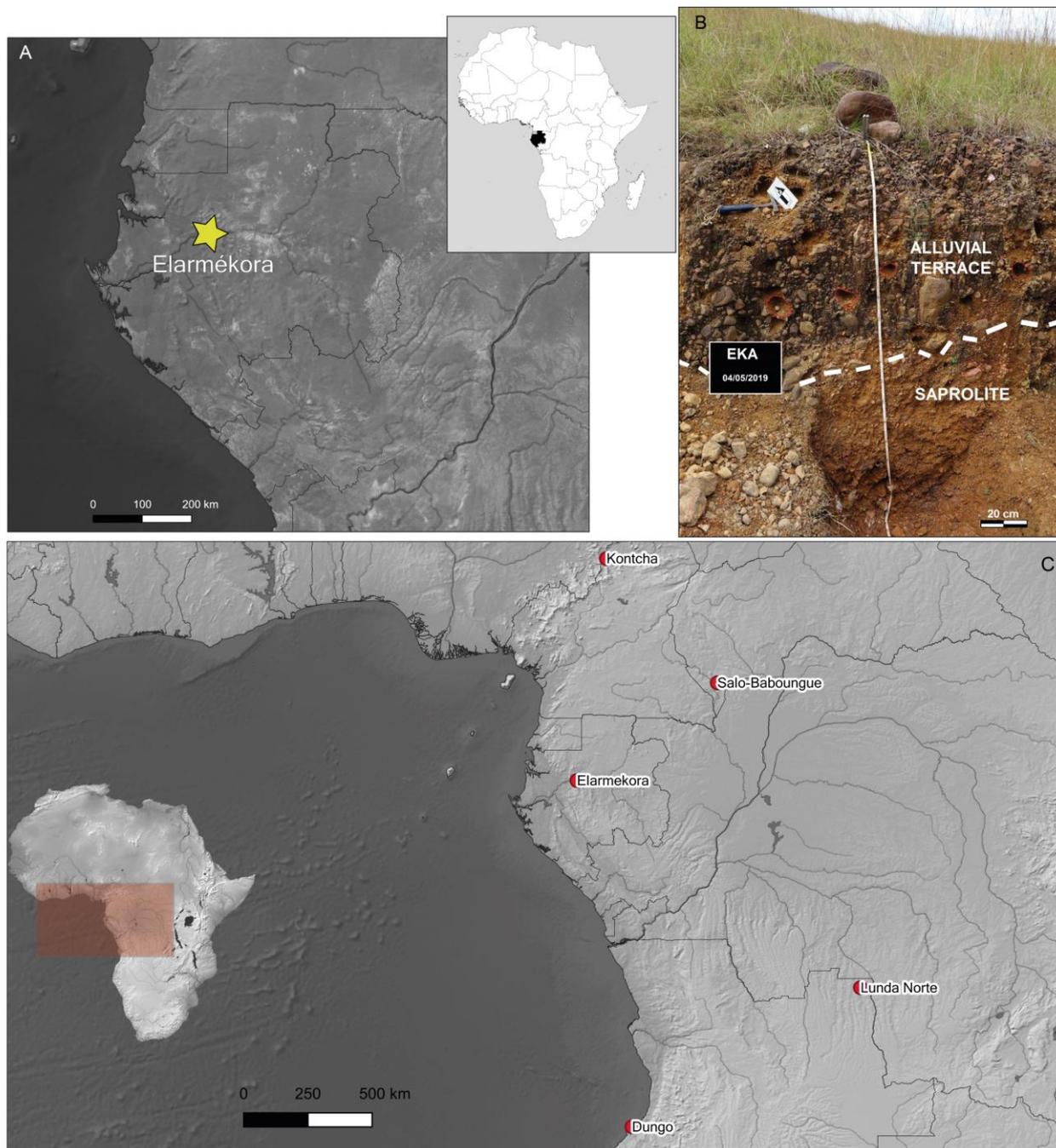
Figure 2 A: Location of Elarmékora in center of Gabon. B: Picture of the alluvial terrace overlying the autochthonous saprolite. C: Map of western Central Africa and location of the sites mentioned in the text.

To better constrain the chronology of this site, possibly the oldest in Atlantic Central Africa, reinvestigations at Elarmékora aimed to identify the timing of this terrace formation, undertaken within the framework of the CAWHFI (Central Africa World Heritage Forest Initiative) program (UNESCO). To do so, several samples were collected for dating by *in situ* produced cosmogenic nuclides ^{10}Be ($T_{1/2}$=1.387±0.012 My [30], [31]) and ^{26}Al ($T_{1/2}$=0.717±0.017 My [32]). This approach is now widely used but has never been attempted in such hostile conditions: at low latitude which reduces the production rate, on a stable craton environment with potential high inheritance implying potential difficulties for dating multiple exposure histories, and lithic artifacts close to the surface with potential continuous exposure. Usually lithic artifacts dated by burial dating

are completely or mostly shielded from cosmic rays since their deposition, allowing radioactive decay of ^{26}Al and ^{10}Be [33], [34], [35].

Samples (quartz pebbles or coarse sand (see Table 1)) were collected during two field campaigns in May 2018 and May 2019. In 2018, samples were collected along a vertical profile from the surface down to 140 cm (in the alluvial material from 0 to 100 cm, then in the saprolite; Fig.2-B) and three surface samples (S1, S2 and S3) were collected at the surface in the herbaceous formation. Two lithic artifacts were collected at the interface of the alluvial deposit and the saprolite to be dated (EKA 18-Outil 1 and EKA18-Outil 2). Both artifacts are quartzite cobble tools: EKA18-Outil 1 is 9 cm long and presents unifacial centripetal removals associated with a disto-lateral retouched edge, and EKA18-Outil 2 is a partially shaped tool with a pointed distal part. Regarding the technological features described in the section below, these artifacts correspond to a core-tool and shaped tool respectively. Interpretation of the 2018 results were quite difficult due to the unexpected nuclide concentration variability within the deposit (only two samples within the saprolite evidenced an exponential decrease), therefore a second field trip was organized in 2019; the same depth profile was re-sampled but a bit deeper (195 cm). One lithic artifact, EKA19-90 has been collected at the interface of the alluvial deposit and the saprolite; this is a quartzite angular cobble. First, a distal surface is used as a flaking surface for centripetal sequence of removals. Second, a disto-lateral sequence of bifacial invasive retouch is shaping a bevel suggesting EKA 19 is a core-tool.

Finally, a 1 m deep depth profile was excavated in the autochthonous formation on top of the hill, just above the alluvial deposit.

Description of stone artifacts

The assemblage of Elarmékora is composed of 14 artifacts (Fig.1, Fig.3) presenting clear intentional anthropic modifications: all artifacts have several regular and large removals with clear negative bulbs and the removal orientations indicate clear flaking strategies (e.g. bidirectional, unidirectional, centripetal) [36]. These artifacts were first described as Early Acheulean in [29] based on a classic typological approach. However, it is now broadly acknowledged that ESA lithic assemblages reveal much more variable hominin behaviors than previously stated, both during the Early and the Middle Pleistocene [15,37–39] and that typological approaches provide few insights into lithic assemblage variability [40]. Consequently, we considered it necessary to revisit the artifacts and reassess their primary techno-cultural affiliation. To do so, we conducted a qualitative technological analysis and made a diacritical sketch for each artifact, grouping the removals in distinct sequences according to their orientation [41,42]. However, all of the pieces are slightly rolled, making it difficult to precisely determine the removal chronology on every piece. The dominant raw material is quartzite which was used on three types of blanks: morphologically homogeneous flat cobbles, angular cobbles and large flakes (>10 cm) detached from large blocks.

Due to the small number of artifacts (n=14), it is difficult to establish a robust techno-typology of the assemblage. We identified two main categories of artifacts, the shaped tools (n=6) – characterized by unstandardized removals aiming to modify the shape of the blank – and the core-tools (n=6) – characterized

by core shaping and a recurrence in the morphology and modality of removals, which may suggest intentional flake production prior to retouching [43,44]. These artifacts were identified along with one raw unmodified large and thick flake and one core presenting two sequences of unidirectional removals. All detailed measurements, weight and additional attributes are presented in a supplementary file (Supp. Table 1) along with supplementary photographs (Supp. Fig. 1). Medium-to-small sized flakes and debris are absent from the assemblage. Indeed, we must consider this assemblage as influenced by the sorting of larger artifacts in the deposit. However, among the shaped tool and core-tool groups, we could observe some repetitive technological and morphometrical features, suggesting an important homogeneity in the production of these artifacts. The assemblage of Elarmékora is characterized by the production of massive heavy-duty tools by using cobble blanks, taking advantage of their natural morphologies.

The shaped tools (n=6, length: $\bar{X}$=138.2mm, sd=26.4; width: $\bar{X}$=89.7mm, sd=11.2; thickness $\bar{X}$=59.7mm, sd=18.3) are large tools with a trihedral or rhomboid section from the mesial to the distal, and a proximal pointed tip. These tools present high indices of elongation (length/width: $\bar{X}$=1.53, sd=0.17) and robustness (width/thickness: $\bar{X}$=1.60, sd=0.40) demonstrating their massive character. Their overall morphology echoes the "pick" tool-type [45,46]. These tools are mainly shaped on angular cobbles (n=4). The different flat surfaces of these blanks are used to provide several striking surfaces for shaping. Indeed, we observe that all of the shaped tools present more than two surfaces, with the exception of one cortical flake with partial unifacial shaping (Fig.3-B). It suggests that knappers were not familiar with bifacial symmetry for shaping; instead, they saw an opportunity for using the different natural flat surfaces of the angular cobbles (Fig. 1-C). Consequently, the different surfaces of the tools are partially shaped but we can observe the use of three or more striking surfaces. The peripheral edges are thick and rarely have retouch removals. Among the three retouched shaped tools, two have retouch scars with feather or step terminations (Fig.1-C) while the third tool has bifacial low-angle retouch. We note that thin and long cutting edges are absent from this group.

The core-tools (n=6, length: $\bar{X}$=126.7mm, sd=10.9; width: $\bar{X}$=103.8mm, sd=20.1; thickness $\bar{X}$=61.5mm, sd=6.5) are slightly smaller than shaped tools but the former are larger and thicker. Also, these pieces are much broader (length/width: $\bar{X}$=1.25, sd=0.23) and slightly less robust (width/thickness: $\bar{X}$=1.69, sd=0.32) than shaped tools. Their shape varies from oval to quadrangular and the section is elongated. These artifacts all show a first sequence of removals suggesting flake production through uni- or bidirectional flaking on the lateral edge of a flat cobble. The use of two opposite large and flat cortical striking platforms may echo the use of the bipolar-on-anvil technique (Fig.1-A,B, Fig.3-A,D) [47,48]. Nevertheless, one piece (Fig.3-C) possesses a centripetal sequence of removals on a convex surface of a rounded cobble. The secondary modification of the artifact occurs through retouch sequences. Usually retouch removals aim to modify one or several peripheral cutting edges and exhibit different morphologies: abrupt, low-angle, unifacial, bifacial, invasive or short, continuous or discontinuous. This variability depicts a tendency to regularization of the initial core blank to obtain functional cutting edges.

Figure 3: Stone artifacts from Elarmékora. A, C and D are core-tools. D also has a shaping sequence on the left lateral edge. B is a unifacially and partially shaped tool on a large cortical flake. In [29], artifact A is illustrated as n°6, B as n°7, C as n°4 and D as n°14.

Methods

All samples were crushed, sieved and cleaned with a mixture of HCl and H_2SiF_6. The extraction method ([49]; [50]), for ^{10}Be and ^{26}Al, involves isolation and purification of quartz and elimination of atmospheric ^{10}Be. Exactly 150 µl of a (3025 ± 9) ppm ^9Be solution was added to the decontaminated quartz. Natural content of aluminum was determined by ICP-OES using an ICAP6500 from Thermo. Beryllium and aluminum were subsequently separated from the solution by successive anionic and cationic resin extractions (DOWEX 1X8

then 50WX8) and precipitations. The final precipitates were dried and heated at 800 °C to obtain BeO and Al_2O_3 and finally mixed with niobium (BeO) and silver (Al_2O_3) powders prior to measurements, which were performed at the French AMS National Facility, ASTER, located at CEREGE in Aix-en-Provence. Beryllium data were calibrated directly against the STD11 standard [51] with a $^{10}Be/^{9}Be$ ratio of (1.191 ± 0.013) x 10^{-11}. Aluminum measurements were performed against an in-house standard called SM-Al-11.with $^{26}Al/^{27}Al =$ (7.401 ± 0.064) x 10^{-12} which has been cross-calibrated against the primary standards certified by a round-robin exercise [50]. Analytical uncertainties (reported as 1σ) include uncertainties associated with AMS counting statistics, AMS external error (0.5% for ^{10}Be), chemical blank measurement, and, regarding ^{26}Al, ^{27}Al measurements.

Measurements of chemically processed blank yield ratios on the order of (2.0 ± 0.75) x 10^{-15} for ^{10}Be and (2.0 ± 2.0) x 10^{-15} for ^{26}Al. A sea level high latitude spallation production rate of 4.02 ± 0.32 at. g^{-1} a^{-1} [52] was used and scaled using [53] polynomials. The $^{26}Al/^{10}Be$ production ratio induced by the standardization used at ASTER is 6.61 ± 0.50.

The general equation used to model ^{10}Be and ^{26}Al concentrations considering the three types of particles involved is given by eq. (1):

$$N(x,\varepsilon,t) = \frac{P_n.e^{-\frac{\rho x}{\Lambda_n}}.\left(1-e^{\left(-t\left(\frac{\rho\varepsilon}{\Lambda_n}+\lambda\right)\right)}\right)}{\frac{\rho\varepsilon}{\Lambda_n}+\lambda} + \frac{P_{slow}.e^{-\frac{\rho x}{\Lambda_{slow}}}.\left(1-e^{-t\left(\frac{\rho\varepsilon}{\Lambda_{slow}}+\lambda\right)}\right)}{\frac{\rho\varepsilon}{\Lambda_{slow}}+\lambda} + \frac{P_{fast}.e^{-\frac{\rho x}{\Lambda_{fast}}}.\left(1-e^{-t\left(\frac{\rho\varepsilon}{\Lambda_{fast}}+\lambda\right)}\right)}{\frac{\rho\varepsilon}{\Lambda_{fast}}+\lambda}$$
$$+N(0,\varepsilon_2,\infty).e^{-\lambda t} \text{ (eq.1)}$$

where P_n, $P_{stop.}$ and P_{fast} are the production of neutrons, stopping and fast muons respectively, ρ is the material density, ε is the denudation rate, t is time, Λ_{neut}, $\Lambda_{stop.}$ and Λ_{fast} are the attenuation lengths of neutrons ($150 g/cm^2$), and stopping (1500 g/cm^2) and fast muons (4320 g/cm^2), respectively. The term $N(0,\varepsilon_2,\infty)$ is a potential inheritance coming from a previous exposure at steady state (T= infinite) and with a denudation ε_2. This denudation ε_2 will referred in the following as a paleo denudation rate; as before the deposition event the samples might have undergone different exposure histories, the term ε_2 is allowed to vary among samples. λ is the radioactive decay constant ($\lambda = \ln2/half\text{-}life$). Muon contribution scheme follows [54].

Results and discussion

All data are presented in Table1. Regarding the depth profile samples EKA18 and EKA19 one can observe two groups of data delimited by the interface between the alluvial deposit and the saprolite (Fig. 2B). Within the saprolite (2018 samples EKA18-115-120 and EKA18-140 extended with 2019 samples EKA19-120, EKA19-140, EKA19-150, EKA19-170 and EKA19-190-195) the concentrations clearly follow the expected

exponential decrease due to the attenuation of cosmic rays particles in the Earth material. In the first meters these attenuation lengths are $156 \frac{+13}{-12}$ g/cm^2 for ^{26}Al and $145 \frac{+8}{-6}$ g/cm^2 for ^{10}Be in quartz for neutrons [55]. For EKA19 samples within the saprolite, using a mean density of 2.4 g/cm^3 deduced from individual density measurements, the experimental apparent attenuations are ~162 g/cm^2 for ^{10}Be and ~169 g/cm^2 for ^{26}Al. This thus unambiguously implies that the studied saprolite was always exposed within the first meters and therefore was never deeply buried by the alluvial deposits.

In the alluvial deposit above the interface, concentrations are, at first glance, more randomly distributed for samples from both 2018 and 2019 field campaigns. This was one reason behind sampling the top hill depth profile a bit higher than the alluvial terrace, but in an area without any signs of the deposit that may be the cause of the variability. In fact, at this position, the expected exponential decrease is observed (stars in Figure 4 in the two upper panels). Moreover, when considering the concentrations of the EKA-TH profile, one can see that the exponential decrease of EKA-TH sample concentrations can be extended to the deeper ones within the saprolite (samples mentioned above); this is represented by the black line in Figure 4 in the two upper panels.

Considering ^{26}Al/^{10}Be ratios, one can observe (Fig. 4 C and D) that they are quite homogenous within the saprolite and more scattered above the interface, with some values that may indicate a complex burial history (EKA18-0; EKA18-Outil2, EKA18-95).

This confirms again that alluvial disturbance has affected only the upper first meter of the studied surface. Finally, one can also observe in Figure 4 that all sample concentrations above the interface are: (1) higher than the interface concentration (~440 kat/g and 2300 kat/g for ^{10}Be and ^{26}Al respectively) and (2) lower than the top surface concentration (~2300 kat/g and 6800 kat/g for ^{10}Be and ^{26}Al respectively), with the exception of EKA19-90-outil ^{26}Al concentration. These observations suggest that all samples may have thus evolved *in situ* and that the first meter has been subsequently perturbed that may be potentially link to biological activity [56], [57] or, may be the results of a strong event that has dismantled an old indurated ferricrust whose relicts can be observed in the field (see Supp Figure 2 and 3).

All these observations being made, the big challenge is to date this surface in order to have at least a minimum age for the found artifacts.

Based on our data descriptions, it was decided that four models should be performed to better bracket the most probable exposure age. All models are based on the depth profile approach [58], [59]. Although the approach of Hidy et al. [59] has been developed on amalgamated samples, it can also be applied on single clasts even though inheritance may be less homogeneous for clasts. Using this single nuclide approach for the first time is interesting to see if both ^{10}Be and ^{26}Al outputs agree.

The Monte Carlo approach of [59] has thus been performed on samples that lie on the exponential decrease shown on Fig.4 considering: (a) the depth profile from saprolite samples only, (b) on a depth profile considering the maximum of samples that are near the exponential decrease curve, (c) the "top hill" depth

profile samples, and finally (d) on a composite profile grouping the saprolite and the "top hill" samples (a and c).

Table 1: Sample positions and measured ^{10}Be, ^{26}Al and ^{27}Al concentrations. Topographic shielding factor for all samples is 1. All samples were prepared at CEREGE and measured on ASTER AMS (see text).

Sample	Type	Depth	Latitude	Longitude	Alt.	^{10}Be	^{26}Al	R(^{26}Al/^{10}Be)	Natural ^{27}Al
		cm	°	°	m	kat/g	kat/g		ppm
EKA18 -0	Quartz pebble	0				2312 ± 41	6663 ± 538	2.88 ± 0.24	3.59 ± 0.07
EKA18 -20	Quartz pebble	20				1390 ± 29	6942 ± 354	4.99 ± 0.28	18.68 ± 0.37
EKA18 -40	Quartz pebble	40				1410 ± 27	5586 ± 560	3.96 ± 0.4	16.46 ± 0.33
EKA18 -60	Quartz pebble	60				776 ± 16	4777 ± 320	6.15 ± 0.43	20.1 ± 0.4
EKA18 -75-80	Coarse gravel	77				912 ± 19	2187 ± 306	2.4 ± 0.34	3.3 ± 0.07
EKA18 -Outil 1	Quartzite cobble	90	-0.09408	11.17027	226	1576 ± 27	7183 ± 318	4.56 ± 0.22	14.33 ± 0.29
EKA18 -Outil 2	Quartzite cobble	90				1077 ± 20	2786 ± 329	2.59 ± 0.31	12.29 ± 0.25
EKA18 -95	Quartz cobble	95				1433 ± 29	2765 ± 223	1.93 ± 0.16	2.76 ± 0.06
EKA18 115-120	Coarse gravel	117				251 ± 8	1717 ± 302	6.85 ± 1.22	22.99 ± 0.46
EKA18 -140	Coarse gravel	140				147 ± 5	928 ± 179	6.33 ± 1.24	15.84 ± 0.32
EKA18 - S1	Quartz cobble	0				710 ± 14	3484 ± 456	4.9 ± 0.65	1.64 ± 0.03
EKA18 - S2	Quartz cobble	0	-0.09296	11.17063	240	920 ± 20	4619 ± 248	5.02 ± 0.29	3.93 ± 0.08
EKA18 - S3	Quartz cobble	0				469 ± 12	2756 ± 227	5.88 ± 0.51	14.27 ± 0.29
EKA19 - 0	Quartz cobble	0				851 ± 153	4682 ± 140	5.5 ± 1.01	19.57 ± 0.39
EKA19 -20	Coarse gravel	20				1253 ± 26	5583 ± 170	4.46 ± 0.16	25.02 ± 0.5
EKA19 -50	Quartz pebble	50				1334 ± 27	6313 ± 213	4.73 ± 0.19	17.44 ± 0.35
EKA19 -70	Quartz pebble	70				1254 ± 27	5782 ± 196	4.61 ± 0.19	15.52 ± 0.31
EKA19 -90 Q Roulé	Quartz cobble	90				1349 ± 29	4508 ± 147	3.34 ± 0.13	25.52 ± 0.51
EKA19 -100	Quartz pebble	100	-0.09408	11.17027	226	983 ± 28	3602 ± 114	3.67 ± 0.16	15.22 ± 0.3
EKA19 -120	Quartz pebble	120				295 ± 8	2014 ± 86	6.84 ± 0.34	13.14 ± 0.26
EKA19 -140	Coarse gravel	140				203 ± 7	1307 ± 61	6.44 ± 0.37	16.47 ± 0.33
EKA19 -150	Coarse gravel	150				195 ± 6	1315 ± 62	6.75 ± 0.38	20.91 ± 0.42
EKA19 -170	Coarse gravel	170				135 ± 5	889 ± 43	6.56 ± 0.39	16.27 ± 0.33
EKA19-190-195	Coarse gravel	192.5				101 ± 3	746 ± 74	7.41 ± 0.77	13.16 ± 0.26
EKA19-90-outil	Quartzite cobble	90				2118 ± 39	9095 ± 272	4.29 ± 0.15	6.04 ± 0.12
EKA-HT -0	Coarse gravel	0				2169 ± 40	7478 ± 225	3.45 ± 0.12	13.94 ± 0.28
EKA-HT -30	Coarse gravel	30				1039 ± 21	5336 ± 177	5.13 ± 0.2	11.36 ± 0.23
EKA-HT -50	Coarse gravel	50	-0.09305	11.17057	257	754 ± 23	4704 ± 185	6.24 ± 0.31	13.35 ± 0.27
EKA-HT -70	Coarse gravel	70				605 ± 14	3416 ± 141	5.64 ± 0.27	11.76 ± 0.24
EKA-HT -90	Coarse gravel	90				442 ± 13	2306 ± 89	5.21 ± 0.26	13.72 ± 0.27

Table 2: Model outputs. The first number is the age (ka) and the second the denudation rate (m/Ma). For all simulations inheritance is negligible.

Profile	^{10}Be		^{26}Al		^{10}Be and ^{26}Al	
	Min (T/ε)	Max (T/ε)	Min (T/ε)	Max (T/ε)	Min (T/ε)	Max (T/ε)
Saprolite sample	663/0	999/0.31	470/0	526/0.05	627/0	720/0.2
Max. samples	674/0	1017/0.44	460/0	558/0.23	620/0	730/0.25
Hill Top	772/0	1179/0.4	457/0	988/0.98	512/0.9	Infinite/0.95
Composite (saprolite samples + Hill Top)	772/0	1180/0.4	482/0	529/0.1	700/0.22	1018/ 0.72

Outputs can be observed in Table 2; all exposure ages (minimum or maximum) determined by ^{26}Al are always lower than those determined by ^{10}Be. Considering ^{10}Be and ^{26}Al separately, the overall maximum and minimum ages for the EKA profiles (alluvial deposit and/or saprolite samples, "top hill" profile not included) range from 456.4 to 1017 ka.

For the same selected profiles, a model based on eq. 1, combining the two nuclides has been also performed using an Excel spreadsheet. For all samples a unique exposure time (t) and a unique denudation rate (ε) after the deposition event have been considered but paleo denudation rates (ε2) were considered as free parameters for each sample. Uncertainties were determined following [60] using the chi square plus one.

Combining the two nuclides allows reducing the time span from 620 ka to 730 ka and denudation rates from 0 to 0.25 m/Ma for the alluvial deposit and/or saprolite samples.

For all simulations, inheritance can be neglected when considering samples close to the exponential decrease.

Considering the three lithic artifacts totally shielded from cosmic rays, their concentrations yield minimum burial ages (no post production) of close to 300 ka for EKA18-Outil 1 and EKA19-90-Outil and close to 1.4 Ma for EKA18-Outil2 with palaeo-denudation rates within the range of 0.45 to 0.7 m/Ma. EKA18-Outil 2 clearly has a complex exposure history or was produced on a previously buried cobble.

One has to be resigned and accept the fact that the minimum age of these artifacts is that of the deposit they belong to, i.e. 620 ka, and that no direct age can be determined.
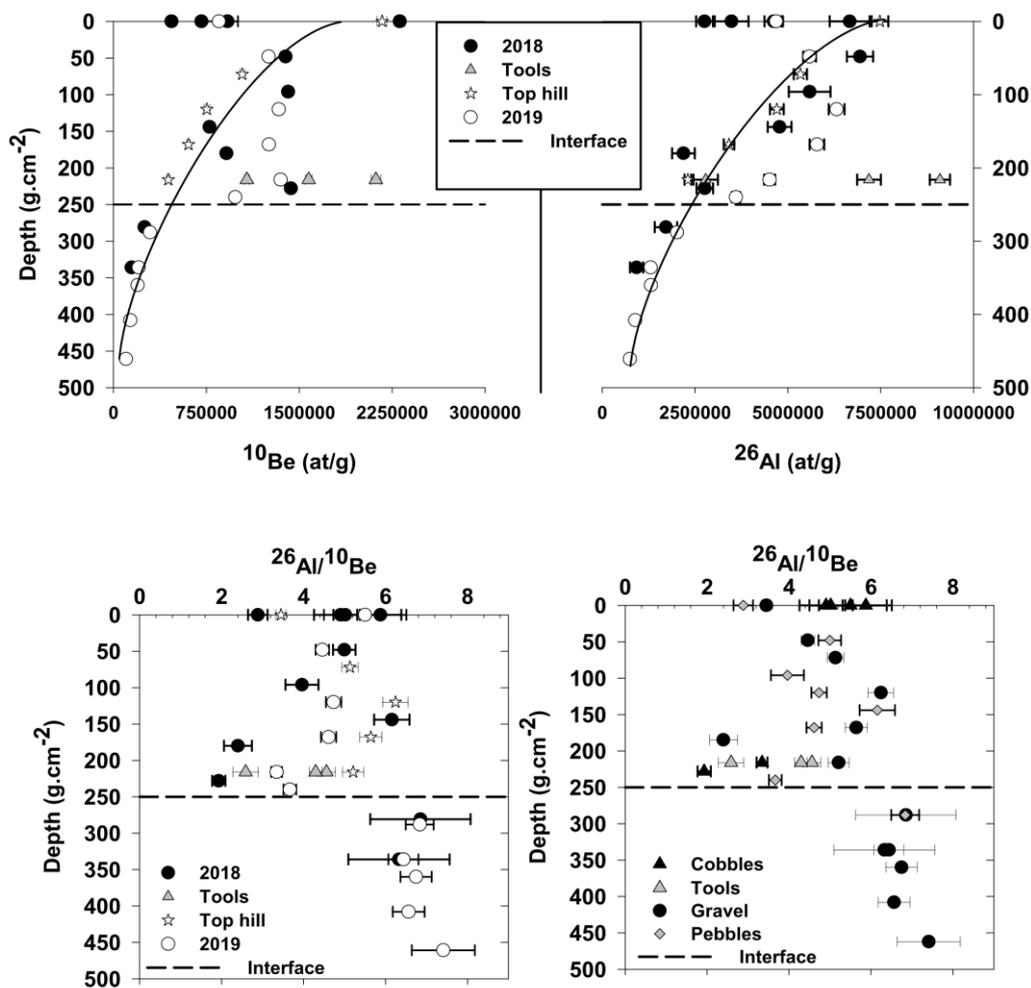
Figure 4: 10Be (panel A), 26Al (panel B) and 26Al/10Be ratio (panel C and D) as a function of depth for EKA18, EKA19 and TH samples. Panel D presents the ratios as a function of sample types (Cobbles (including tools), pebbles and gravels. Dashed line represents the interface between the alluvial deposit and the saprolite (see Fig 2B) and the black line shows the exponential decrease due to neutron attenuation in the penetrated material (see text).

The same dating difficulties arose in Angola [28] where lithic remains were found buried in a sandy matrix whose age was determined to be close to 650 ka, contemporaneous with the Elarmékora site. However, the Angolan artifacts were buried deeper (~3 m) and have buried ages ranging from 0.7 to 2 Ma but as for Elarmékora, the minimum age to be trusted is the matrix age they belong to.

While few archaeological studies have been done in western Africa, the minimum age of 620 ka falls just after the mid-Pleistocene transition [61], [62] coincident with the onset and intensification of high-latitude glacial cycles [63]. These climatic changes, probably coupled with tectonic activity, have been identified in other parts of Africa and seems to have impacted faunal populations [64],[65],[66],[67],[68].

When considering the technological patterns of the Elarmékora lithic assemblage, we face a difficulty in its classification. On the one hand, the large flake production evidenced by two artifacts and the presence of a pick tool-type may echo the Acheulean techno-complex which is contemporary to Elarmékora and more broadly prevails in sub-Saharan Africa during the early Middle Pleistocene [10–12,46,69]. On the other hand,

some typical Acheulean technical patterns such as Large Cutting Tools, bifacial shaping and specific tool types such as cleavers, handaxes or polyhedra are absent from the Elarmékora assemblage. A shaping strategy is present but it never involves the use of bifacial symmetry for guiding the reduction sequence. In addition, the types of flaking strategies identified at Elarmékora may not be associated with a specific time period or any techno-cultural entity as these are pan-chronological features. Overall, in the Elarmékora assemblage we identified both general technological affinities with the Acheulean techno-complex and specific local technical features, such as exploiting the natural volumetric advantages of the pebbles, the 'multifacial' shaping and the close relationship between cores and pebble tools. Consequently, due to these specific patterns and to the small size of the assemblage, we now may consider the lithic technology of Elarmékora as an "undiagnostic ESA". Finally, this site provides data on ESA technology in the equatorial belt of Central Africa which may, in the future, contribute to refining our understanding of the specific role of equatorial regions in human evolution [70,71].

So far, only the site of Dungo in Angola presents ages that converge with those of Elarmékora, dated by cosmogenic nuclides to ca. 600–650 ka. The technological patterns of Dungo also suggest a dominance of pebble and cobbles tools (Fig.5-B) along with some shaped tool production [72,73]. Similar patterns have been reported from a number of undated ESA sites in western Central Africa (Fig.2-C), among which are the Lunda-Norte sites in north-eastern Angola [74]. Comparable technological trends have been observed on other Central African ESA sites such as Baboungué in the Sangha River Basin in Central African Republic (Fig.5-A) [23] and Kontcha in Cameroon [75]. While these remain undated, the site of Kontcha offers good characteristics for applying the same cosmogenic dating methods as those used here, since it is located on a high alluvial terrace covered with a lateritic cuirass which is elevated more than 35 m above the Mayo Deo River.

Despite the current lack of hominin fossils in western sub-Saharan Africa, the convergence of the Elarmékora ages with the sites of Dungo in Angola, is remarkable because for the first time we can glimpse a new hominin dispersal scenario. To confirm this "West Side Story", more dateable sites are necessary to refine the chronology of early human dispersals and to provide inter-site lithic comparison to better understand local technical trajectories during the Middle Pleistocene.

Conclusion

The significance of this discovery lies in the fact that it is the first time that an Earlier Stone Age site has been dated on the Atlantic edge of the Congo Basin, a vast region where research is not developed due to dense forest cover which does not promote accessibility and complicates logistics.

Despite hostile climatic conditions that prevent the good conservation of open-air Pleistocene sites, the lithic artifacts discovered in the alluvial deposit of Elarmékora have been dated at minimum as old as 650 ka by the used of cosmogenic ^{10}Be and ^{26}Al pairs. This minimum age falls just at the end of a major climatic change, the mid-Pleistocene transition, observed throughout the world. The atypical lithic assemblage of Elarmékora points toward a specific Earlier Stone Age technology in western Congo Basin. Even though the assemblage needs to be enlarged, we presented technical specificities which raise questions on the origins of these populations, on the relationships between the contemporary Acheulean technology which prevails on a large part of Africa during the mid-Pleistocene Transition and on the potential adaptation of the tool-kits in the equatorial belt.

This study confirms the antiquity of the hominin presence in western Central Africa more than 3500 km away from the closest hominin fossil sites in South Africa. It shows a tremendous advance in our knowledge of the evolution of our ancestors which could upset the models established and could provide the first evidence of a "West Side Story" for early hominins dispersal within Africa.
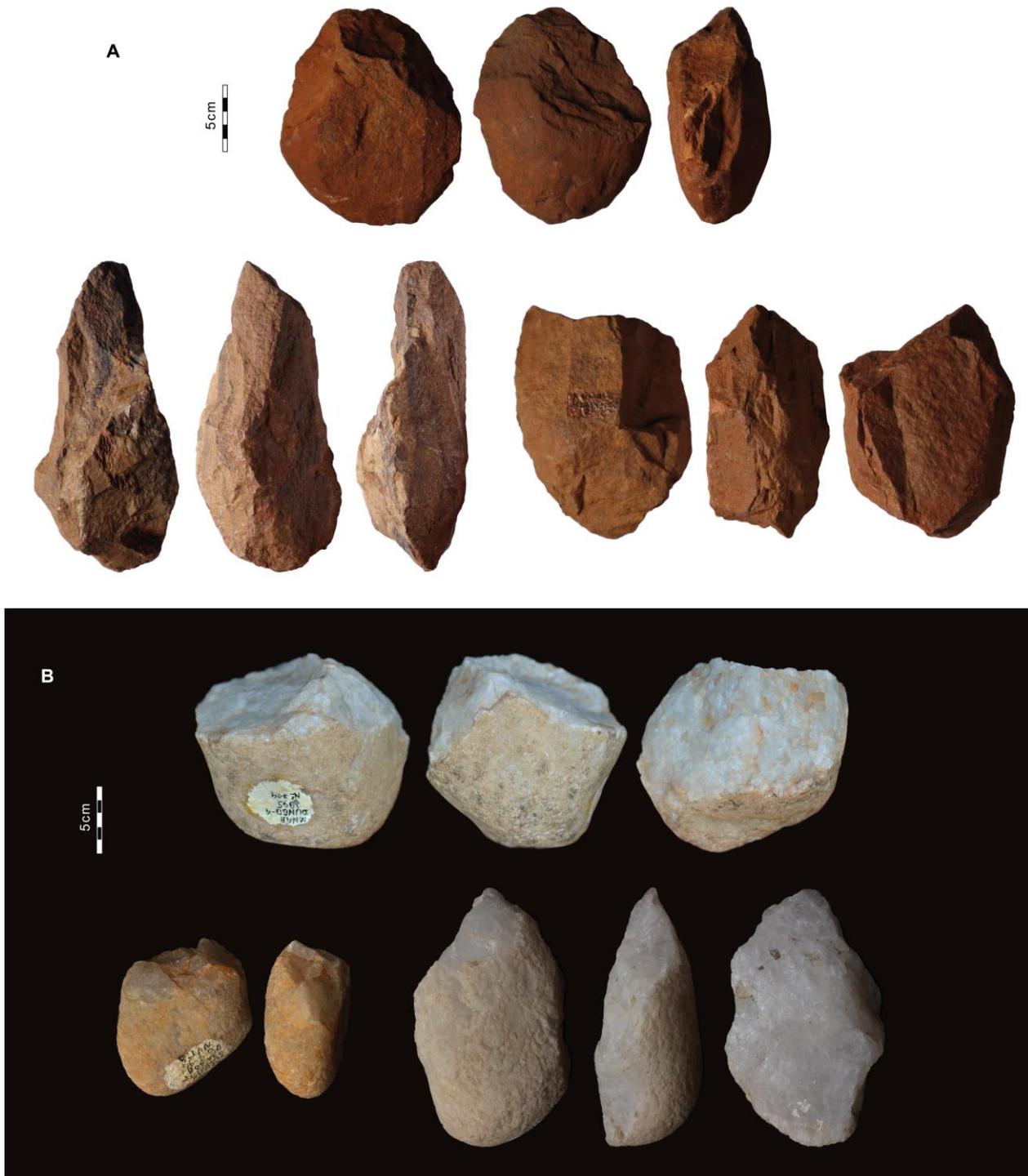
Figure 5 : A: ESA Artifacts from Baboungué, Central African Republic. B: ESA artifacts on pebbles and cobbles from Dungo IV.

Funding

References

1. Harmand S *et al.* 2015 3.3-million-year-old stone tools from Lomekwi 3, West Turkana, Kenya. *Nature* **521**, 310–315.(DOI: 10.1038/nature14464)

2. Hublin J-J *et al.* 2017 New fossils from Jebel Irhoud, Morocco and the pan-African origin of Homo sapiens. *Nature* **546**, 289–292. (DOI:10.1038/nature22336)

3. De Weyer L. 2020 *Les premières traditions techniques du Paléolithique ancien*. Eva David. L'Harmattan. ISBN : 978-2-343-21324-8

4. Wentworth CK. 1922 A scale of grade and class terms for clastic sediments. *The Journal of Geology* **30**, 377–392. https://www.jstor.org/stable/30063207

5. Braun DR *et al.* 2019 Earliest known Oldowan artifacts at> 2.58 Ma from Ledi-Geraru, Ethiopia, highlight early technological diversity. *Proceedings of the National Academy of Sciences* **116**, 11712–11717. (DOI:10.1073/pnas.1820177116)

6. Toth N, Schick K. 2018 An overview of the cognitive implications of the Oldowan Industrial Complex. *Azania: Archaeological Research in Africa* **53**, 3–39.(doi : 10.1080/0067270X.2018.1439558)

7. McPherron SP. 1994 A reduction model for variability in Acheulian biface morphology. *Dissertations available from ProQuest* , 1–433.

8. Gallotti R, Mussi M. 2018 Before, During, and After the Early Acheulean at Melka Kunture (Upper Awash, Ethiopia): A Techno-economic Comparative Analysis. In *The Emergence of the Acheulean in East Africa and Beyond* (eds R Gallotti, M Mussi), pp. 53–92. Cham: Springer International Publishing. (DOI: 10.1007/978-3-319-75985-2_4)

9. Sharon G. 2009 Acheulian Giant-Core Technology: A Worldwide Perspective. *Current Anthropology* **50**, 335–367. (DOI:10.1086/598849)

10. Leakey MD. 1971 Olduvai Gorge, Excavations in Beds I and II, 1960–1963, vol. 3. *Cambridge: Cambridge Univ. Press.* DOI:10.1017/S0079497X00012226

11. Kuman K. 2019 Acheulean Industrial Complex. In *Encyclopedia of Global Archaeology*, pp. 1–12. Cham: Springer International Publishing. ISBN 978-1-4419-0466-9

12. Sharon G. 2010 Large flake Acheulian. *Quaternary International* **223**, 226–233. DOI:10.1016/j.quaint.2009.11.

13. Sharon G. 2007 *Acheulian Large Flake Industries: Technology, Chronology, and Signifiance*. BAR International Series. Oxford. ISBN-13: 978140730143.

14. de la Torre I. 2016 The origins of the Acheulean: past and present perspectives on a major transition in human evolution. *Phil. Trans. R. Soc. B* **371**, 20150245. (DOI:10.1098/rstb.2015.0245)

15. Douze K *et al.* 2021 A West African Middle Stone Age site dated to the beginning of MIS 5: Archaeology, chronology, and paleoenvironment of the Ravin Blanc I (eastern Senegal). *Journal of Human Evolution* **154**, 102952. doi : 10.1016/j.jhevol.2021.102952

16. Alsdorf D *et al.* 2016 Opportunities for hydrologic research in the Congo Basin. *Reviews of Geophysics* **54**, 378–409. doi : 10.1002/2016RG000517

17. White F. 1986 *La végétation de l'Afrique*. ORSTOM-UNESCO.

18. Taylor N. 2016 Across Rainforests and Woodlands: A Systematic Reappraisal of the Lupemban Middle Stone Age in Central Africa. In *Africa from MIS 6-2* (eds SC Jones, BA Stewart), pp. 273–299. Dordrecht: Springer Netherlands. ISBN: 978-94-017-7519-9

19. Schwartz D. 1996 Archéologie préhistorique et processus de formation des stone-lines en Afrique Centrale (Congo-Brazzaville et zones periphiques). *Geo-Eco-Trop* **10**, 15–38. https://horizon.documentation.ird.fr/exl-doc/pleins_textes/pleins_textes_6/b_fdi_47-48/010011752.pdf

20. Mercader J, Martí R, Martínez JL, Brooks A. 2002 The nature of 'stone-lines' in the African quaternary record: archaeological resolution at the rainforest site of Mosumu, Equatorial Guinea. *Quaternary International* **89**, 71–96. doi : 10.1016/S1040-6182(01)00082-9

21. Stoops G. 1990 The stone-line as a key to former surface processes: an example 2709910225, from the lower Zaïre. In *Paysages quaternaires de l'Afrique centrale atlantique*, ISBN 9782709910224

22. de Bayle des Hermens R, Oslisly R, Peyrot B. 1987 Premières séries de pierres taillées du Paléolithique inférieur découvertes au Gabon, Afrique centrale. *L'Anthropologie* **91**, 693–698.

23. de Bayle des Hermens R. 1973 Recherches préhistoriques en République Centrafricaine. Thèse de doctorat, Muséum national d'Histoire naturelle, Aix-en-Provence.

24. Cahen D. 1975 *Le site archéologique de La Kamoa (Région du Shaba, République du Zaire) de l'Age de la Pierre Ancien à l'Age du Fer*. Annales sciences humaines. Tervuren: Musée royal de l'Afrique centrale.

25. Lanfranchi R, Clist B. 1991 *Aux origines de l'Afrique centrale*. Sepia. ISBN 10: 2907888110 / ISBN 13: 9782907888110

26. Ervedosa C. 1980 *Arqueologia angolana*. Edições 70.

27. Nenquin J. 1967 Contributions to the Study of the Prehistoric Cultures of Rwanda and Burundi. PhD Thesis, Musée Royal de l'Afrique Centrale - Annales - Série IN N°8, Tervuren.

28. Lebatard AE, Bourlès DL, Braucher R. 2019 Absolute dating of an Early Paleolithic site in Western Africa based on the radioactive decay of in situ-produced 10Be and 26Al. *Nuclear Instruments and Methods in Physics Research, Section B: Beam Interactions with Materials and Atoms* **456**, 169–179. (DOI:10.1016/j.nimb.2019.05.052)

29. Oslisly R, Peyrot B. 1992 Un gisement du Paleolithique inferieur: la haute terrasse d'Elarmekora - moyenne vallee de l'Ogooue (Gabon). Problemes chronologiques et paleogeographiques. *Comptes Rendus - Academie des Sciences, Serie II* **314**, 309–312.

30. Korschinek G *et al.* 2010 A new value for the half-life of 10Be by Heavy-Ion Elastic Recoil Detection and liquid scintillation counting. *Nuclear Instruments and Methods in Physics Research Section B: Beam Interactions with Materials and Atoms* **268**, 187–191. (DOI:10.1016/j.nimb.2009.09.020)

31. Chmeleff J, von Blanckenburg F, Kossert K, Jakob D. 2010 Determination of the 10Be half-life by multicollector ICP-MS and liquid scintillation counting. *Nuclear Instruments and Methods in Physics Research Section B: Beam Interactions with Materials and Atoms* **268**, 192–199. (DOI:10.1016/j.nimb.2009.09.012)

32. Samworth EA, Warburton EK, Engelbertink GAP. 1972 Beta Decay of the $^{26}\mathrm{Al}$ Ground State. *Physical Review C* **5**, 138–142. (DOI:10.1103/PhysRevC.5.138)

33. Granger DE, Muzikar PF. 2001 Dating sediment burial with in situ-produced cosmogenic nuclides: theory, techniques, and limitations. *Earth and Planetary Science Letters* **188**, 269–281. (DOI:10.1016/S0012-821X(01)00309-0)

34. Granger D. 2006 A Review of Burial Dating Methods Using 26Al and 10Be. *Geological Society of America Special Paper* **415**. (DOI:10.1130/2006.2415(01))

35. Wang K, Xu X, Sun X, Tu H, Zeng Q, Lu Y, Lu H, Wang S. 2019 Cosmogenic nuclide burial dating of Liuwan Paleolithic site in the Luonan Basin, Central China. *Journal of Geographical Sciences* **29**, 406–416. (DOI:10.1007/s11442-019-1606-1)

36. Niang K. 2014 Le Mode 1 en Italie entre hétérogénéité et géofacts : le cas de la redéfinition technologique de l'industrie lithique du site de Bel Poggio. *L'Anthropologie* **118**, 391–407. (DOI:10.1016/j.anthro.2014.10.004)

37. Schick K, Clark JD. 2003 Biface technological development and variability in the Acheulean industrial complex in the Middle Awash region of the Afar Rift, Ethiopia. *Multiple approaches to the study of bifacial technologies* , 1–30. ISBN 1-931707-42-1

38. Harmand S. 2009 Variability in raw material selectivity at the late Pliocene sites of Lokalalei, West Turkana, Kenya. In *Interdisciplinary approaches to the Oldowan*, pp. 85–97. Springer. DOI: 10.1007/978-1-4020-9060-8_8

39. Gowlett JAJ. 2015 Variability in an early hominin percussive tradition: the Acheulean versus cultural variation in modern chimpanzee artefacts. *Philosophical Transactions of the Royal Society B: Biological Sciences* **370**, 20140358. (DOI:10.1098/rstb.2014.0358)

40. Boëda E. 2013 *Techno-logique & Technologie. Une préhistoire des objets lithiques.* @rchéo-éditions. Paris. ISBN 978-2-36461-004-0

41. Dauvois M. 1976 Precis de Dessin Dynamique et Structural des Industries Lithiques Préhistoriques. Fanlac, Périgueux, 263 p. *Dynamic and Structural Drawing precise of Prehistoric Lithic Industries"*

42. Mesfin I, Pleurdeau D, Forestier H. 2021 L'assemblage lithique du site Acheuléen de Namib IV (Namib central, Namibie). *L'Anthropologie* **125**, 102848. (DOI:10.1016/j.anthro.2021.102848)

43. Shea JJ, editor. 2020 Cores and Core-Tools. In *Prehistoric Stone Tools of Eastern Africa: A Guide*, pp. 137–164. Cambridge: Cambridge University Press. DOI**:** 10.1017/9781108334969

44. McPherron SP. 2009 *Tools versus Cores: Alternative Approaches to Stone Tool Analysis*. Cambridge Scholars Publishing. ISBN 1-84718-117-1

45. Gao X, Guan Y. 2018 Handaxes and the Pick-Chopper Industry of Pleistocene China. *Quaternary International* **480**, 132–140. (DOI:10.1016/j.quaint.2017.03.051)

46. Clark JD. 2001 *Kalambo Falls Prehistoric Site, III: The Earlier Cultures: Middle and Earlier Stone Age*. Cambridge University Press, Cambridge. DOI:10.1017/S0003598X00090712

47. Soriano S, Robert A, Huysecom E. 2010 Percussion bipolaire sur enclume: choix ou contrainte? L'exemple du Paléolithique d'Ounjougou (Pays dogon, Mali). *PALEO. Revue d'archéologie préhistorique* , 123–132. DOI: 10.4000/paleo.1962

48. Guyodo J-N, Marchand G. 2005 La percussion bipolaire sur enclume dans l'Ouest de la France de la fin du Paléolithique au Chalcolithique : une lecture économique et sociale. *Bulletin de la Société préhistorique française* **102**. (DOI:10.3406/bspf.2005.13141)

49. Braucher R *et al.* 2000 Application of in situ-produced cosmogenic ^{10}Be and ^{26}Al to the study of lateritic soil development in tropical forest: Theory and examples from Cameroon and Gabon. *Chemical Geology* **170**. (DOI:10.1016/S0009-2541(99)00243-0)

50. Merchel S, Bremser W. 2004 First international 26Al interlaboratory comparison - Part I. *Nuclear Instruments and Methods in Physics Research, Section B: Beam Interactions with Materials and Atoms* **223–224**, 393–400. (DOI:10.1016/j.nimb.2004.04.076)

51. Braucher R, Guillou V, Bourlès DL, Arnold M, Aumaître G, Keddadouche K, Nottoli E. 2015 Preparation of ASTER in-house 10Be/9Be standard solutions. *Nuclear Instruments and Methods in Physics Research, Section B: Beam Interactions with Materials and Atoms* **361**, 335–340. (DOI:10.1016/j.nimb.2015.06.012)

52. Borchers B *et al.* 2016 Geological calibration of spallation production rates in the CRONUS-Earth project. *Quaternary Geochronology* **31**, 188–198. (DOI:10.1016/j.quageo.2015.01.009)

53. Stone JO. 2000 Air pressure and cosmogenic isotope production. *Journal of Geophysical Research: Solid Earth* **105**, 23753–23759. (DOI:10.1029/2000JB900181)

54. Braucher R, Merchel S, Borgomano J, Bourlès DL. 2011 Production of cosmogenic radionuclides at great depth: A multi element approach. *Earth and Planetary Science Letters* **309**. (DOI:10.1016/j.epsl.2011.06.036)

55. Brown ET, Brook EJ, Raisbeck GM, Yiou F, Kurz MD. 1992 Effective attenuation lengths of cosmic rays producing 10Be AND 26Al in quartz: Implications for exposure age dating. *Geophysical Research Letters* **19**, 369–372. (DOI:10.1029/92GL00266)

56. Brown ET, Stallard RF, Larsen MC, Raisbeck GM, Yiou F. 1995 Denudation rates determined from the accumulation of in situ-produced 10Be in the luquillo experimental forest, Puerto Rico. *Earth and Planetary Science Letters* **129**, 193–202. (DOI:doi : 10.1016/0012-821X(94)00249-X)

57. Braucher R, Colin F, Brown ET, Bourlès DL, Bamba O, Raisbeck GM, Yiou F, Koud JM. 1998 African laterite dynamics using in situ-produced 10Be. *Geochimica et Cosmochimica Acta* **62**, 1501–1507. (DOI:10.1016/S0016-7037(98)00085-4)

58. Braucher R, Del Castillo P, Siame L, Hidy AJ, Bourlés DL. (2009). Determination of both exposure time and denudation rate from an in situ-produced 10Be depth profile. *Quaternary Geochronology* **4**, 56–67. (DOI:10.1016/j.quageo.2008.06.001)

59. Hidy AJ, Gosse JC, Pederson JL, Mattern JP, Finkel RC. 2010 A geologically constrained Monte Carlo approach to modeling exposure ages from profiles of cosmogenic nuclides: An example from Lees Ferry, Arizona. *Geochemistry, Geophysics, Geosystems* **11**. (DOI:10.1029/2010GC003084)

60. Bevington PR, Robinson DK. 2003 *Data reduction and error analysis for the physical sciences*. Mc Graw-Hill. ISBN: 9780072472271

61. deMenocal PB. 2004 African climate change and faunal evolution during the Pliocene-Pleistocene. *Earth and Planetary Science Letters* **220**, 3–24. (DOI:10.1016/S0012-821X(04)00003-2)

62. Clark P, Archer D, Pollard D, Blum J, Rial J, Brovkin V, Mix A, Pisias N, Roy M. 2006 The Middle Pleistocene transition: characteristics, mechanisms, and implications for long-term changes in atmospheric pCO2. *Quaternary Science Reviews* **25**, 3150–3184. (DOI:10.1016/j.quascirev.2006.07.008)

63. Owen RB *et al.* 2018 Progressive aridification in East Africa over the last half million years and implications for human evolution. *Proceedings of the National Academy of Sciences of the United States of America* **115**, 11174–11179. (DOI:10.1073/pnas.1801357115)

64. Vrba ES. 1995 The fossil record of African antelopes (Mammalia, Bovidae) in relation to human evolution and paleoclimate. In *Paleoclimate and Evolution, with Emphasis on Human Origins.* (ed LH Vrba E.S., DentonG.H., Partridge, T.C., and Burckle), pp. 385–424. New Haven. ISBN-13: 978-0300063486

65. Potts R et al. 2018 Environmental dynamics during the onset of the Middle Stone Age in in eastern Africa. 90, 86–90. DOI: 10.1126/science.aao2200

66. Behrensmeyer AK, Potts R, Deino A. 2018 The Oltulelei Formation of the southern Kenyan Rift Valley: A chronicle of rapid landscape transformation over the last 500 k.y. *Bulletin of the Geological Society of America* **130**, 1474–1492. (DOI:10.1130/B31853.1)

67. Telfer PT *et al.* 2003 Molecular evidence for deep phylogenetic divergence in Mandrillus sphinx. *Molecular Ecology* **12**, 2019–2024. (DOI:10.1046/j.1365-294X.2003.01877.x)

68. Anthony NM *et al.* 2007 The role of Pleistocene refugia and rivers in shaping gorilla genetic diversity in central Africa. *Proceedings of the National Academy of Sciences of the United States of America* **104**, 20432–20436. (DOI:10.1073/pnas.0704816105)

69. Shea JJ, editor. 2020 Stone Tools: Essential Terms and Concepts. In *Prehistoric Stone Tools of Eastern Africa: A Guide*, pp. 14–40. Cambridge: Cambridge University Press.

70. Mercader J. 2002 Forest people: The role of African rainforests in human evolution and dispersal. *Evolutionary Anthropology: Issues, News, and Reviews* **11**, 117–124. (DOI:10.1002/evan.10022)

71. Roberts P. 2019 *Tropical Forests in Prehistory, History, and Modernity*. Oxford University Press. DOI:10.15184/aqy.2020.72

72. da Piedade de Jesus M. 2010 Recherches sur le Paléolithique inférieur de la bande côtière d'Angola. Étude comparative techno-typologique et tracéologique du matériel lithique des sites de Dungo IV, Dungo V et Dungo XII. *Afrique : Archéologie & Arts* , 103–105. https://www.theses.fr/146988671

73. Mesfin I, Lotter MG, Benjamim MH. 2021 A new approach to quantifying raw material selectivity in the African Acheulean: perspectives from Angola and South Africa. *Journal of African Archaeology* (DOI:10.1163/21915784-20210013)

74. Clark JD. 1963 *Prehistoric cultures of northeast Angola and their significance in tropical Africa*. Museu do Dundo.

75. Hervieu J. 1969 Découverte de la Pebble-Culture au Nord de l'Adamaoua (Cameroun). Incidences géomorphologiques et pédogénétiques. *Comptes Rendus de l'Académie des Sciences, D, 268, 2335-2338.* **D**, 2335–2338.

**I/ Lithic artifacts from Elarmekora**

5cm
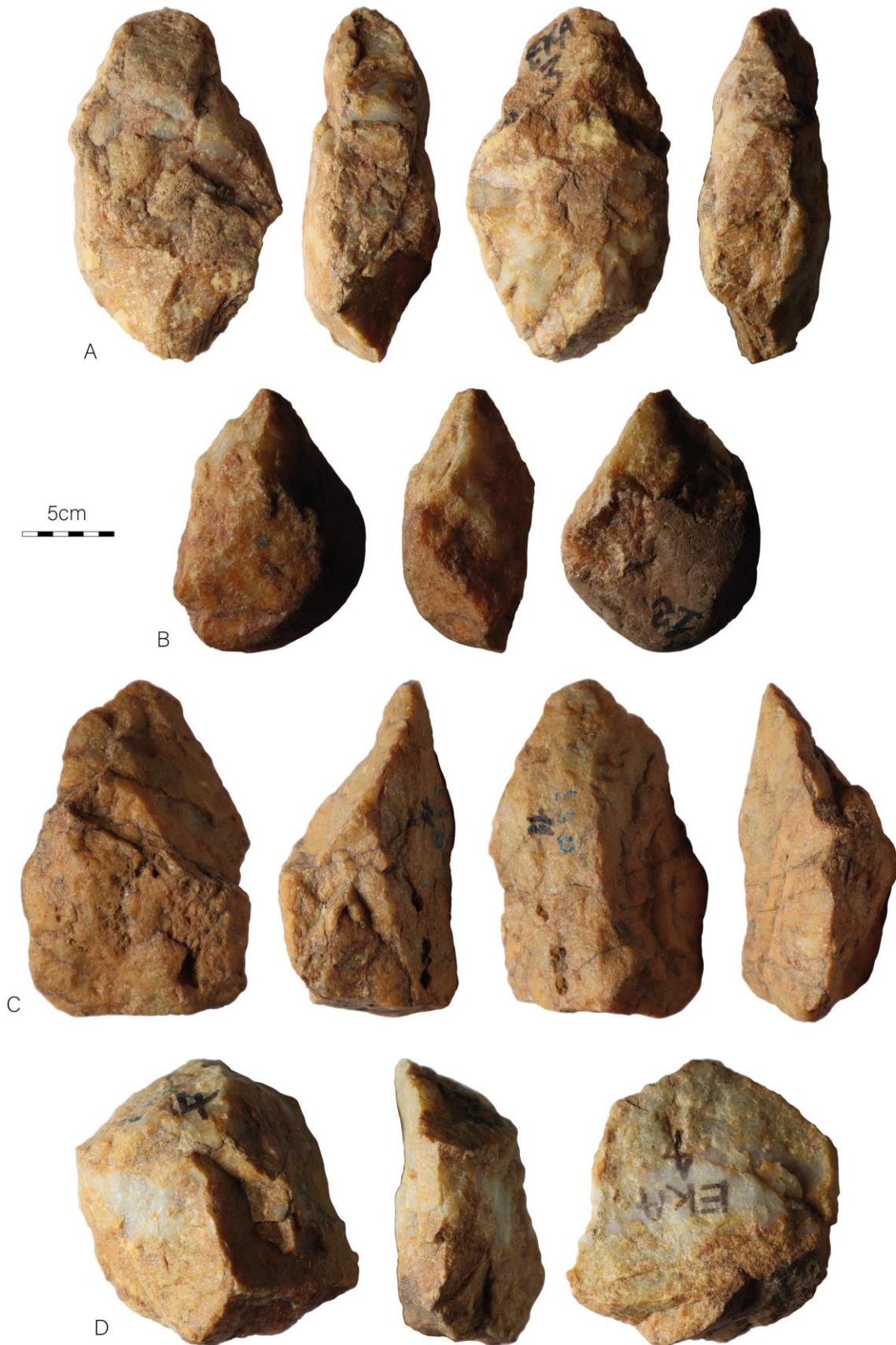
Figure 1 : Lithic artifacts from Elarmekora assemblage. In Oslisly and Peyrot 1992, artifact A is n°12, B is n°11, C is n°10 and D is n°5.

Table 1 : Lithic artefacts database

Num	Length (mm)	Width (mm)	Thickness (mm)	Elongation (l/w)	Robustness (w/t)	Techno-type	Blank	Raw material	Modality	Retouch
EKA1	124	112	52	1.11	2.15	Core tool	Flat cobble	Quartzite-sandstone	Bidirectional peripheral flaking	Lateral rectilinear abrupt retouch
EKA2	122	135	67	0.90	2.01	Core tool	Flat cobble	Quartzite-sandstone	Bidirectional peripheral flaking	Disto-lateral rectilinear abrupt retouch
EKA3	161	91	61	1.77	1.49	Shaped tool	Angular cobble	Quartzite	Quadrifacial partial shaping	Proximal step-termination retouch
EKA4	117	135	66	0.87	2.04	Flake	Undetermined	Quartzite-sandstone	Multidirectional dorsal scars	Absent
EKA5	121	91	62	1.33	1.47	Core tool	Angular cobble	Quartzite	Bidirectional unifacial flaking	Distal notches
EKA6	135	111	67	1.22	1.66	Core tool	Angular cobble	Quartzite-sandstone	Unidirectional unifacial flaking + unifacial partial shaping	Absent
EKA7	131	98	46	1.34	2.13	Shaped tool	Pebble	Quartzite-sandstone	Unifacial partial shaping	Distal bifacial retouch
EKA8	114	77	55	1.48	1.40	Core tool	Flat cobble	Quartzite	Unidirectional unifacial flaking	Lateral rectilinear abrupt retouch
EKA9	129	95	71	1.36	1.34	Core	Angular cobble	Quartzite-sandstone	Unidirectional unifacial flaking	Absent
EKA10	167	102	84	1.64	1.21	Shaped tool	Angular cobble	Quartzite-sandstone	Trifacial partial shaping	Peripheral step-termination retouch
EKA11	151	93	76	1.62	1.22	Shaped tool	Angular bloc	Quartzite	Trifacial partial shaping	Absent
EKA12	121	83	56	1.46	1.48	Shaped tool	Rounded cobble	Quartzite-sandstone	Trifacial partial shaping	Absent
EKA13	144	97	66	1.48	1.47	Core tool	Flat cobble	Quartzite-sandstone	Centripetal flaking	Peripheral lateral abrupt retouch
EKA14	98	71	35	1.38	2.03	Shaped tool	Undetermined	Quartzite	Trifacial partial shaping	Absent

II/ Pictures of the surroundings of Elarmékora terrace.

Figure 2 : Panel A: In the background the Otoumbi mount and a perched terraces equivalent to Elarmekora site. In the foreground the surroundings of the studied site.

Panel B: Close view of the Ogouée River and of the 175 m high terrace at 175m above the river.
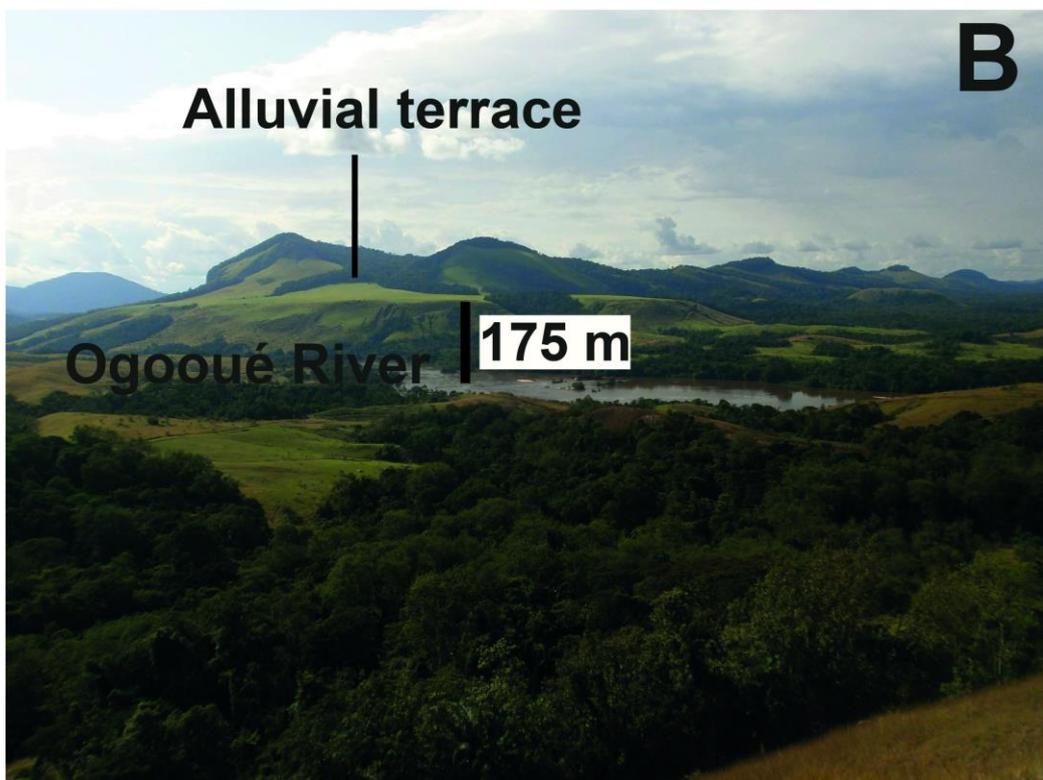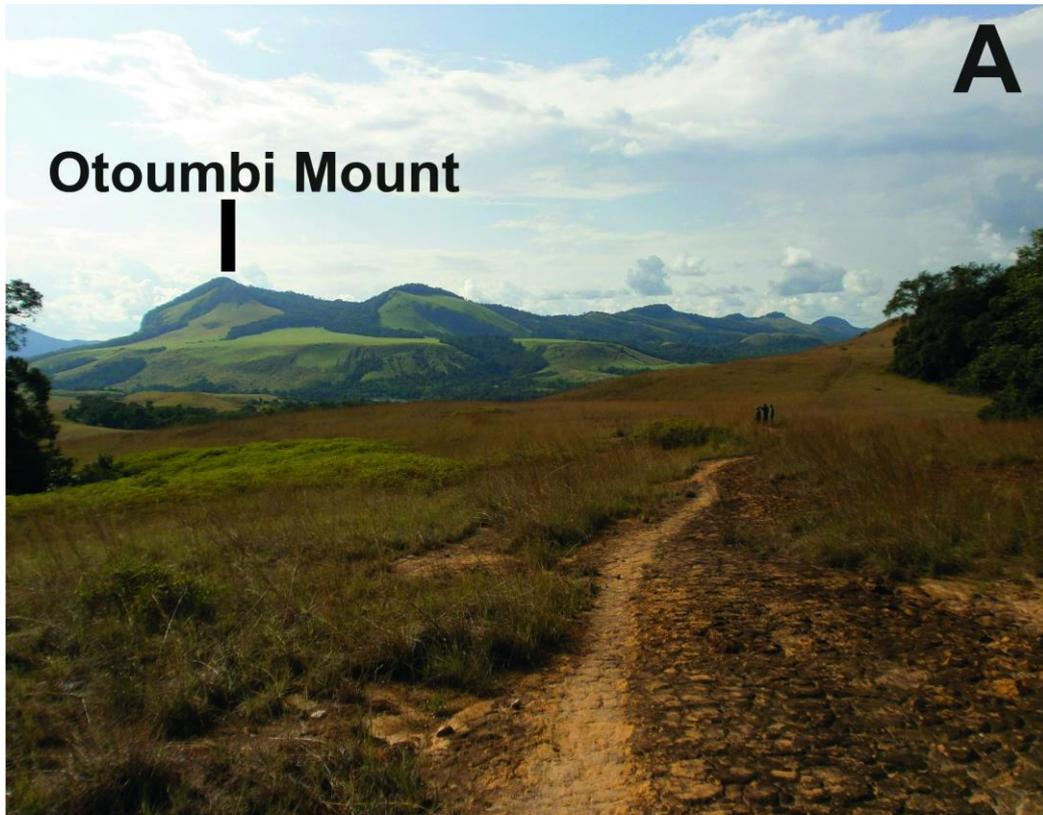
Figure 3: Panel A: Typical surface near the studied site with the presence of rolled cobbles and relicts of ferricrust.

Panel B: Close up on a dismantled indurated ferricrust.

III/ Depth profile modelling.

All models have been performed using the Matlab approach of Hidy et al (2010) with a modified muons scheme for muons based on Braucher et al (2011). Despite Hidy et al. claims that their model is appropriated for amalgamated samples, it has been demonstrated that this approach is also valid on single clasts (Braucher et al. 2009). The main assumption being that the inheritance is the same for all samples.

In order to determine the exposure age of the studied surface several simulation s have been intended:
- Considering only bottom samples only, those within the saprolite below the alluvial deposit.
- Considering the maximum samples that verify the theoretical exponential decrease linked to neutron attenuation.
- Considering only the 1 m deep top hill profile.
- Considering bottom samples only, those within the saprolite below the alluvial deposit combined with the top hill profile

For each model, samples used are indicated in a dedicated table. Only samples lying along an exponential decrease have been considered.

The models considering both ^{10}Be and ^{26}Al have not been performed with Hidy Matlab routine but with an excel approach using eq. 1, one for ^{10}Be and and one for ^{26}Al, both with same exposure time and denudation rate for the period after the deposition event and with variable paleo denudation ($\varepsilon 2$). To determine the uncertainties, the approach of the chi square plus one has been used following Bevington et al (2003).

Note that for all models the inheritance component is negligible; in the excel approach this is described by high values for $\varepsilon 2$.

Production parameters (at/g/yr) used for all models

Spallation 10Be prod.	Spallation 26 Al prod	Slow Muons for 10Be	Fast Muons for 10Be	Slow Muons for ^{26}Al	Fast muons for ^{26}Al
2.84	18.77	0.0107	0.0369	0.7485	0.0766

Main outputs :

Profile	^{10}Be		^{26}Al		^{10}Be and ^{26}Al	
	Min (T/ε)	Max (T/ε)	Min (T/ε)	Max (T/ε)	Min (T/ε)	Max (T/ε)
Saprolite sample	662.66/0	998.7/0.31	469.6/0	526.3/0.05	627/0	720/0.2
Max. samples	674.2/0	1016.6/0.44	459.9/0	557.8/0.23	620/0	730/0.25
Top hill	772.2/0	1179.3/0.4	456.4/0	988.1/0.98	512/0.9	Infinite/0.95
Composite (saprolite samples + Top hill)	772.2/0	1179.8/0.4	482.3/0	528.9/0.1	700/0.22	1018/ 0.72

1- Bottom samples within the saprolite.

| Sample	^{10}Be (at/g)	^{26}Al (at/g)
EKA-115-120	250.57 ± 7.98	1717.14 ± 301.87
EKA19-120	294.7 ± 7.51	2014.51 ± 86.13
EKA19-140	203.09 ± 6.55	1307.49 ± 61.34
EKA19-150	194.96 ± 6	1315.12 ± 62.2
EKA19-170	135.44 ± 4.64	889.12 ± 43.21
EKA19-190-195	100.67 ± 3.26	745.96 ± 73.61

Models outputs for ^{10}Be

```
              | age (ka) | inheritance (10^4 atoms g^-1) | erosion rate (cm ka^-1) | density (g/ccm) |
         mean | 788.930 |                       0.234 |                   0.009 |           2.460 |
       median | 776.227 |                       0.177 |                   0.007 |           2.471 |
         mode | 755.600 |                       0.010 |                   0.010 |           2.499 |
    min chi^2 | 853.216 |                       0.199 |                   0.001 |           2.478 |
      maximum | 998.763 |                       1.469 |                   0.031 |           2.500 |
      minimum | 662.641 |                       0.000 |                   0.000 |           2.260 |
Bayesian most probable | 696.970 |                0.000 |                   0.000 |                 |
Bayesian 2-sigma upper | 968.477 |                1.702 |                   0.069 |                 |
Bayesian 2-sigma lower | 532.429 |                  NaN |                     NaN |                 |
Bayesian 1-sigma upper | 851.557 |                1.010 |                   0.045 |                 |
Bayesian 1-sigma lower | 616.846 |                0.057 |                   0.004 |                 |
```
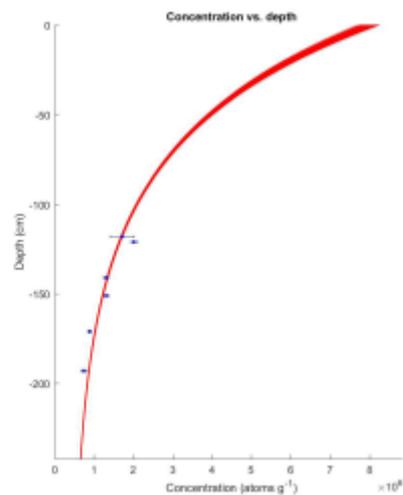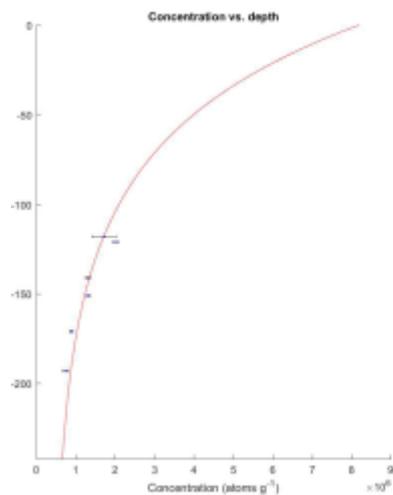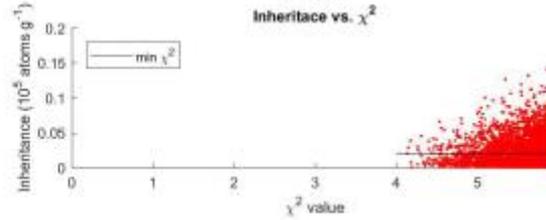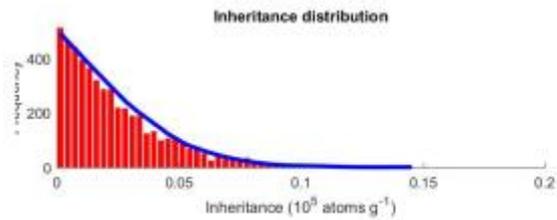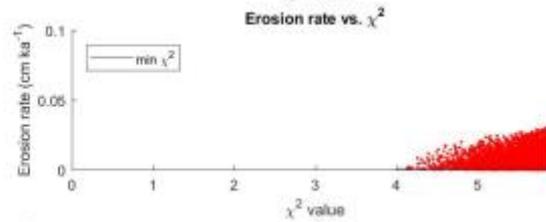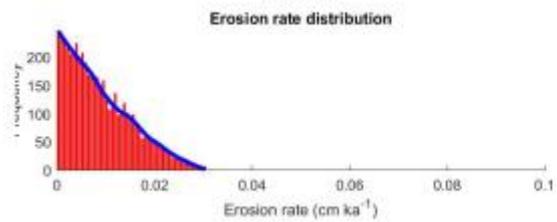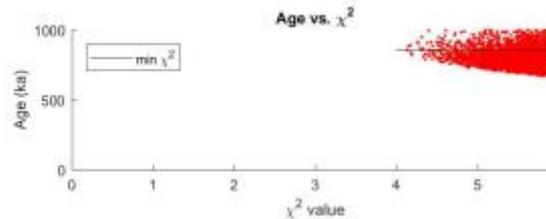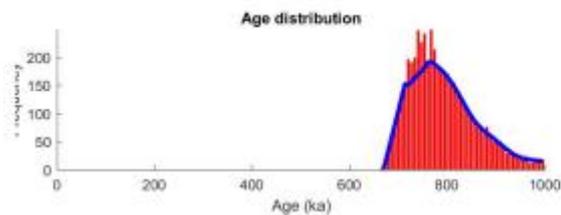

Models outputs for ^{26}Al

	age (ka)	inheritance (10^4 atoms g^-1)	erosion rate (cm ka^-1)	density (g/ccm)
mean	503.437	0.352	0.001	2.466
median	504.523	0.284	0.001	2.472
mode	505.700	0.050	0.000	2.498
min chi^2	515.794	0.002	0.000	2.497
maximum	526.333	1.195	0.005	2.500
minimum	469.658	0.000	0.000	2.373
Bayesian most probable	471.212	0.036	0.001	
Bayesian 2-sigma upper	539.480	1.169	0.005	
Bayesian 2-sigma lower	NaN	NaN	NaN	
Bayesian 1-sigma upper	514.136	0.992	0.004	
Bayesian 1-sigma lower	458.973	0.149	0.001	
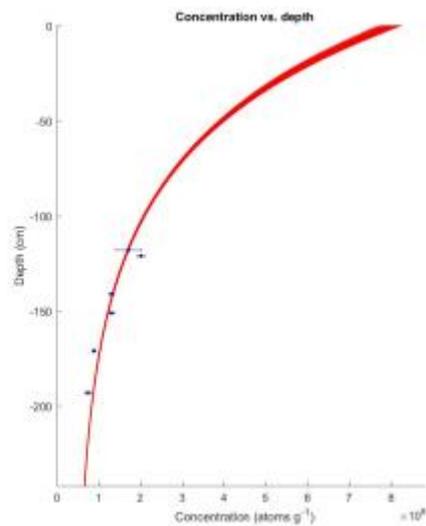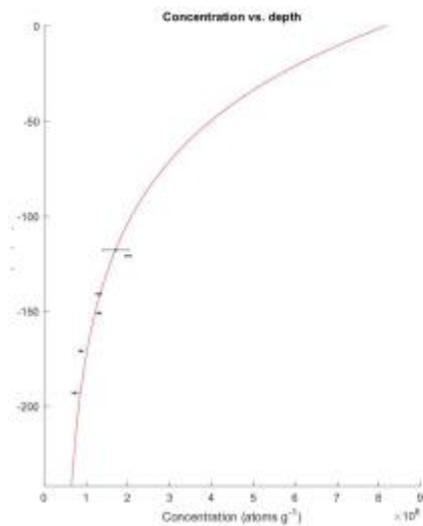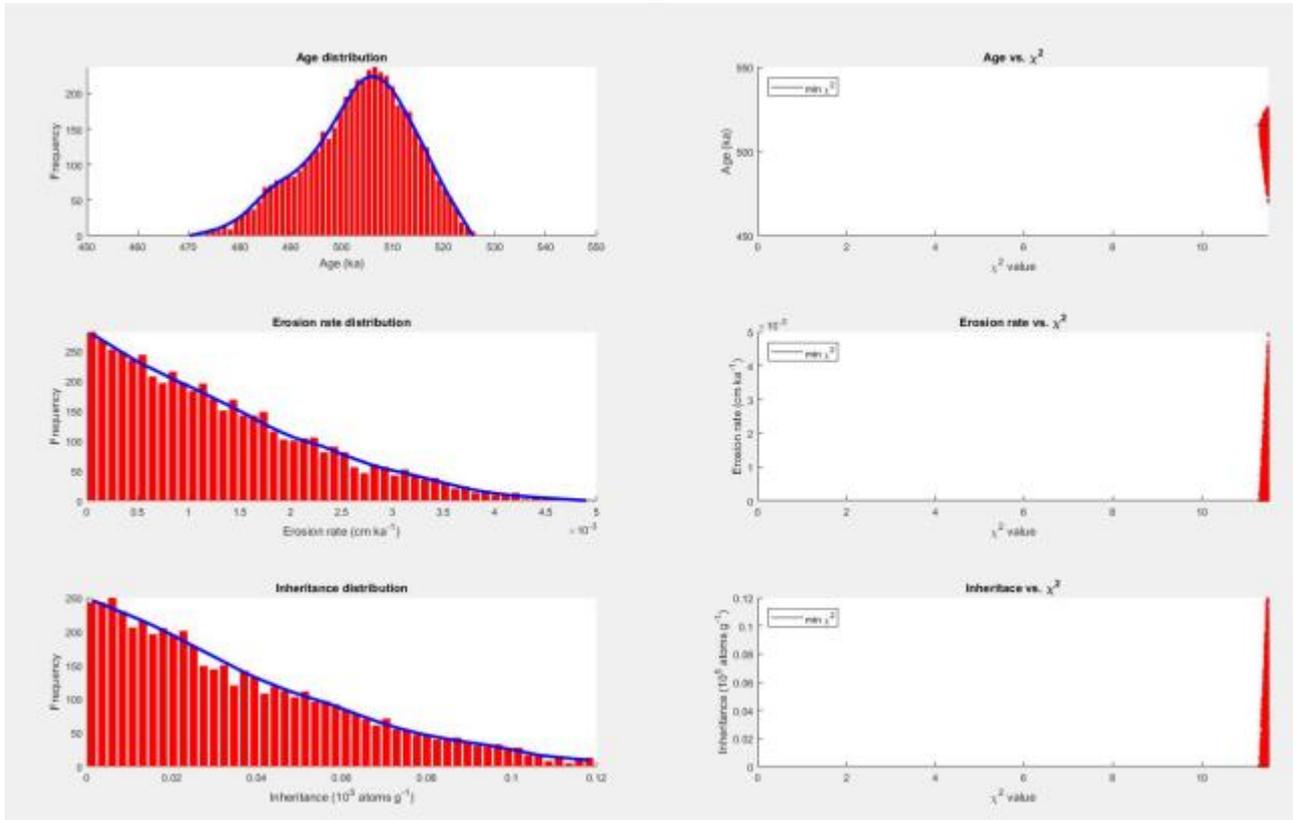
**Model output considering both 10Be and 26Al.**
Ages range between 627 ka to 720 ka with a denudation lower than 0.2 m/Ma.
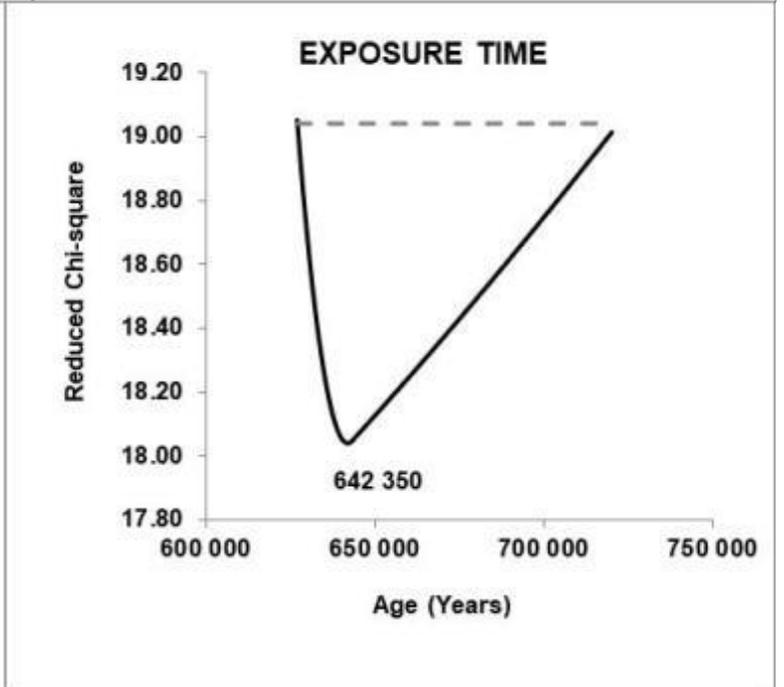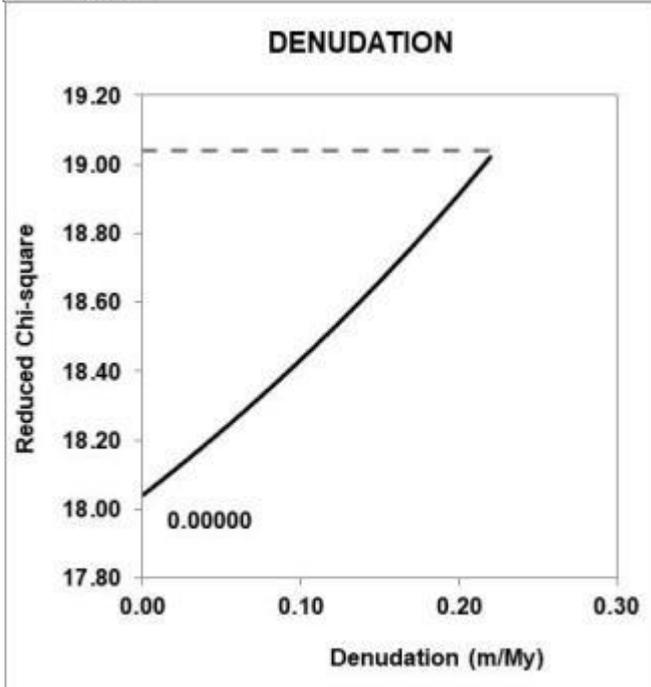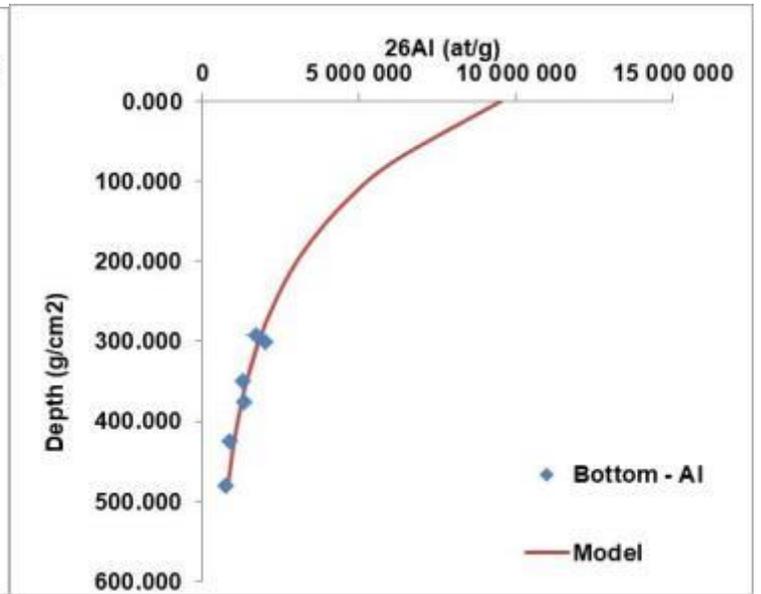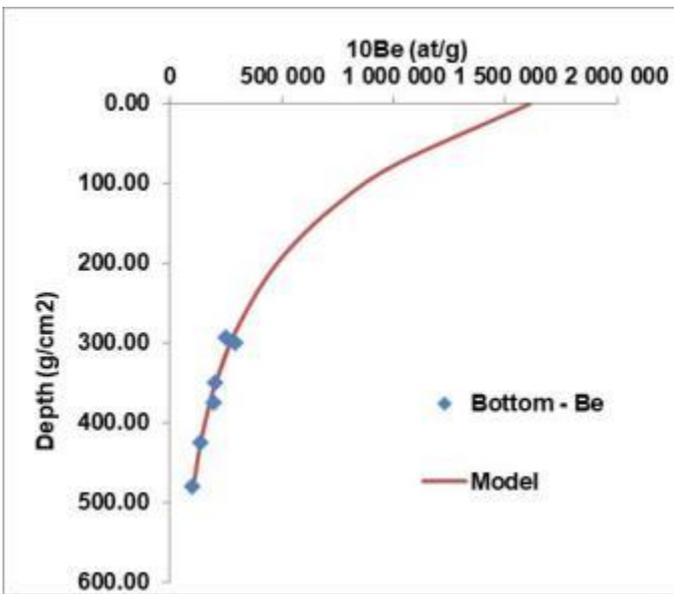
Dash line corresponds to the minimum chi-square plus one equivalent to 1 sigma uncertainty. (Bevington et al. 2003)

2- Model using the maximum of samples that verify the theoretical exponential decrease linked to neutron attenuation.

Sample	10Be (at/g)	26Al (at/g)
EKA-0		6663.13 ± 537.88
EKA-20	1389.96 ± 29.23	6941.8 ± 353.66
EKA19-20	1252.57 ± 25.62	5582.93 ± 170.41
EKA-40		5585.59 ± 559.77
EKA-60	776.12 ± 16.12	4776.55 ± 319.88
EKA-95		2764.75 ± 222.94
EKA-115-120	250.57 ± 7.98	1717.14 ± 301.87
EKA19-120	294.7 ± 7.51	2014.51 ± 86.13
EKA-140	146.6 ± 4.6	927.71 ± 178.87
EKA19-140	203.09 ± 6.55	1307.49 ± 61.34
EKA19-150	194.96 ± 6	1315.12 ± 62.2
EKA19-170	135.44 ± 4.64	889.12 ± 43.21
EKA19-190-195	100.67 ± 3.26	745.96 ± 73.61

Models outputs for 10Be

```
|                          | age (ka) | inheritance (10^4 atoms g^-1) | erosion rate (cm ka^-1) | density (g/ccm) |
|                     mean |  777.363 |                         0.304 |                   0.014 |           2.484 |
|                   median |  764.724 |                         0.249 |                   0.012 |           2.487 |
|                     mode |  733.900 |                         0.060 |                   0.010 |           2.496 |
|                 min chi^2 |  718.148 |                         0.019 |                   0.000 |           2.499 |
|                  maximum | 1016.587 |                         1.179 |                   0.044 |           2.500 |
|                  minimum |  674.231 |                         0.000 |                   0.000 |           2.435 |
| Bayesian most probable   |  733.333 |                         0.000 |                   0.000 |                 |
| Bayesian 2-sigma upper   |  974.749 |                         1.270 |                   0.043 |                 |
| Bayesian 2-sigma lower   |  661.039 |                           NaN |                     NaN |                 |
| Bayesian 1-sigma upper   |  843.225 |                         0.644 |                   0.027 |                 |
| Bayesian 1-sigma lower   |  696.917 |                         0.018 |                   0.002 |                 |
```
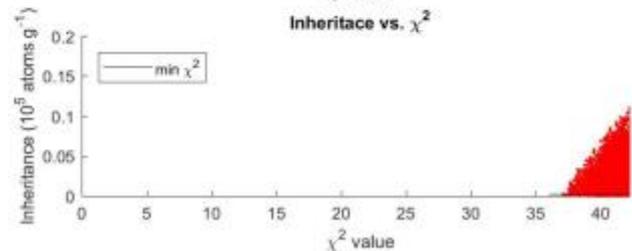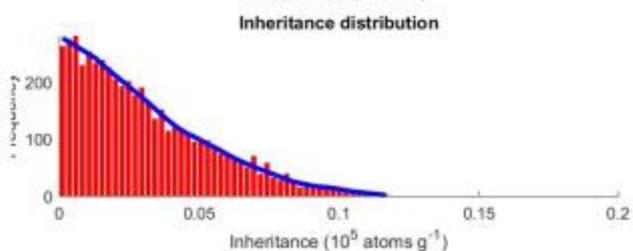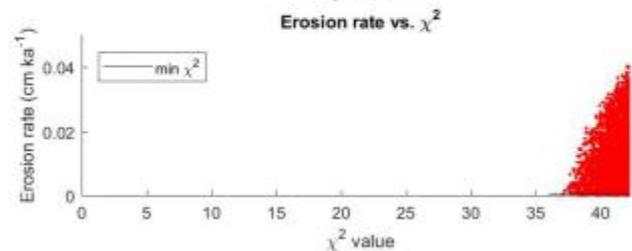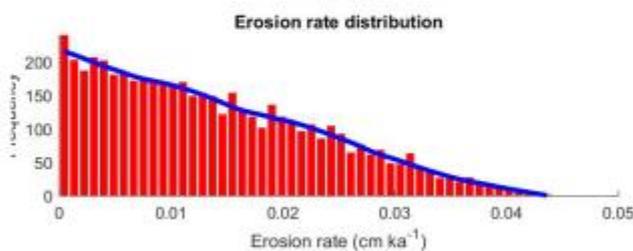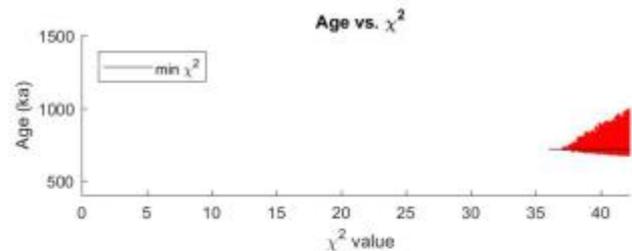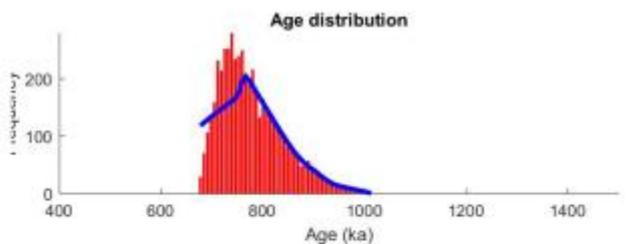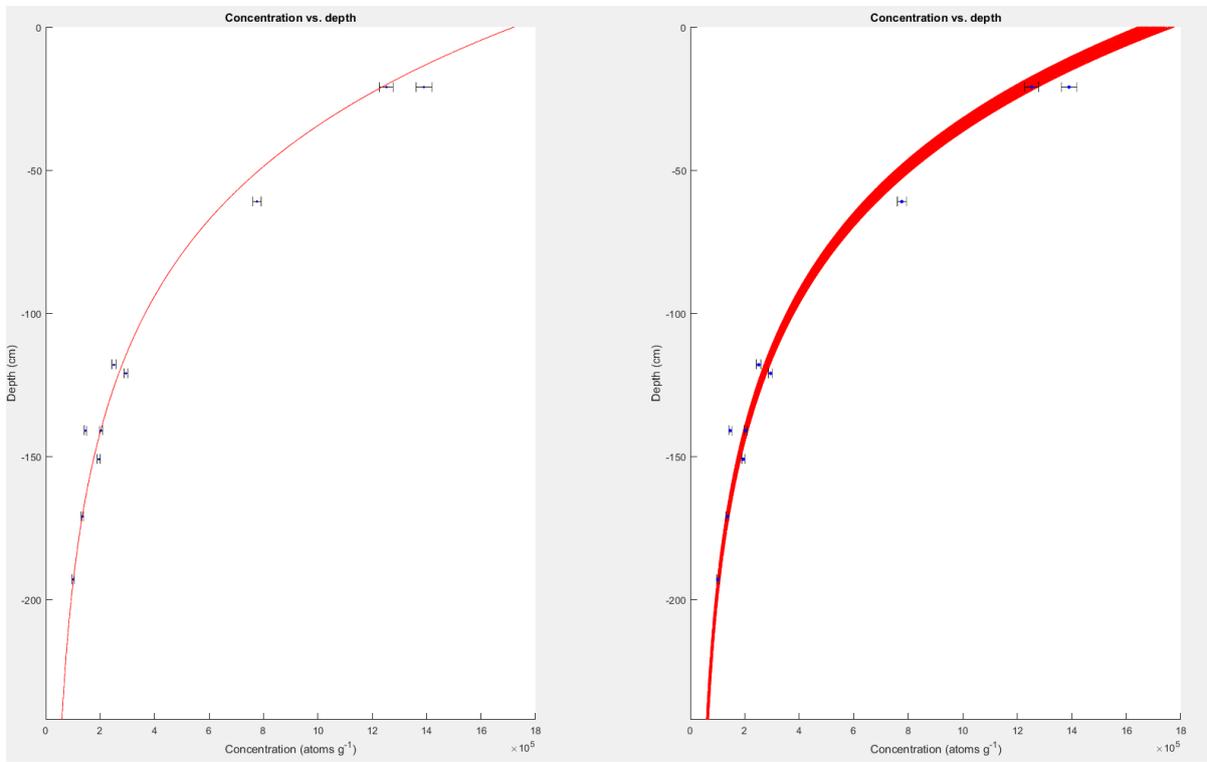
Models outputs for 26Al

	age (ka)	inheritance (10^4 atoms g^-1)	erosion rate (cm ka^-1)	density (g/ccm)
mean	505.080	1.872	0.007	2.430
median	504.888	1.560	0.006	2.437
mode	499.200	0.390	0.010	2.469
min chi^2	492.390	0.218	0.000	2.420
maximum	557.786	6.838	0.023	2.500
minimum	459.957	0.001	0.000	2.295
Bayesian most probable	490.909	0.000	0.001	
Bayesian 2-sigma upper	589.928	9.687	0.029	
Bayesian 2-sigma lower	415.644	NaN	NaN	
Bayesian 1-sigma upper	540.418	7.928	0.025	
Bayesian 1-sigma lower	451.989	1.018	0.004	

Concentration vs. depth / Concentration vs. depth
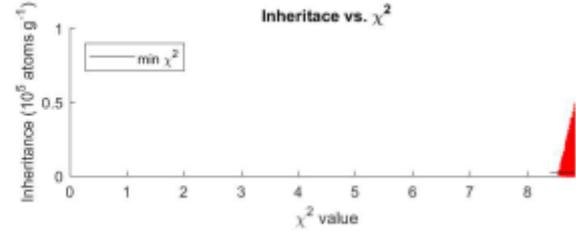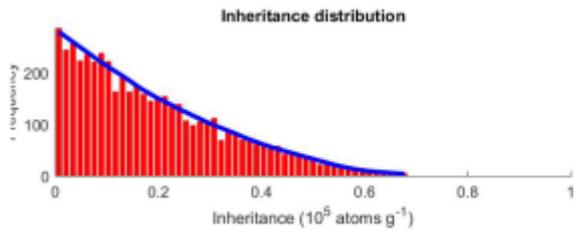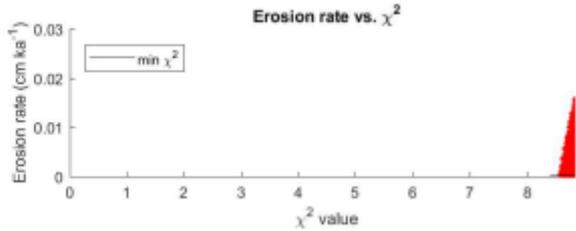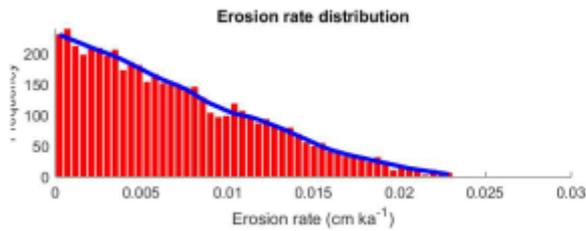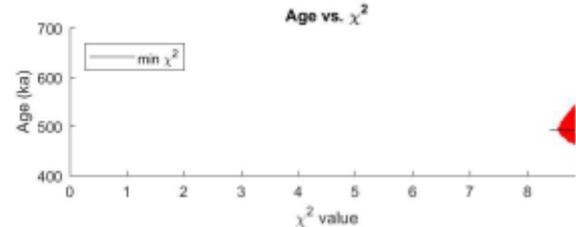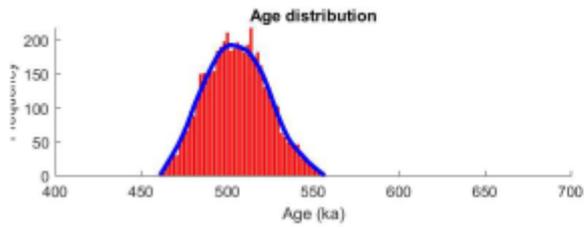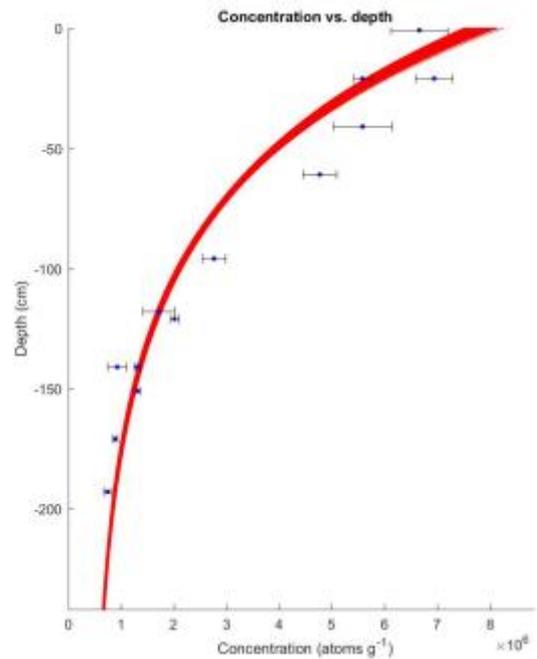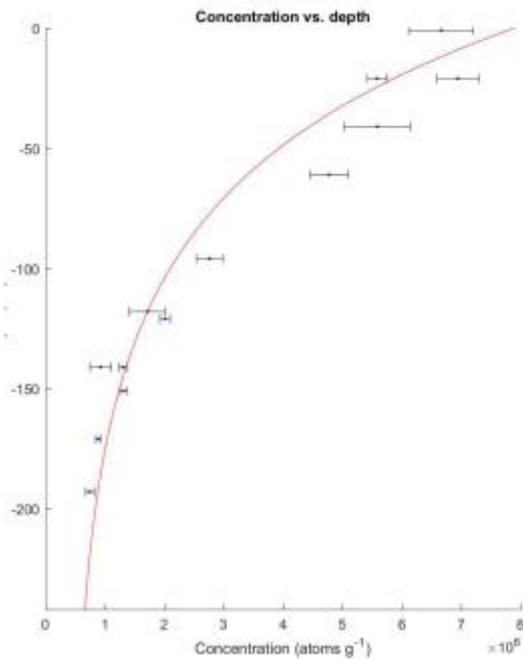
Model output considering both 10Be and 26Al.

Age range between 620 ka to 730 ka with a denudation lower than 0.25 m/Ma.
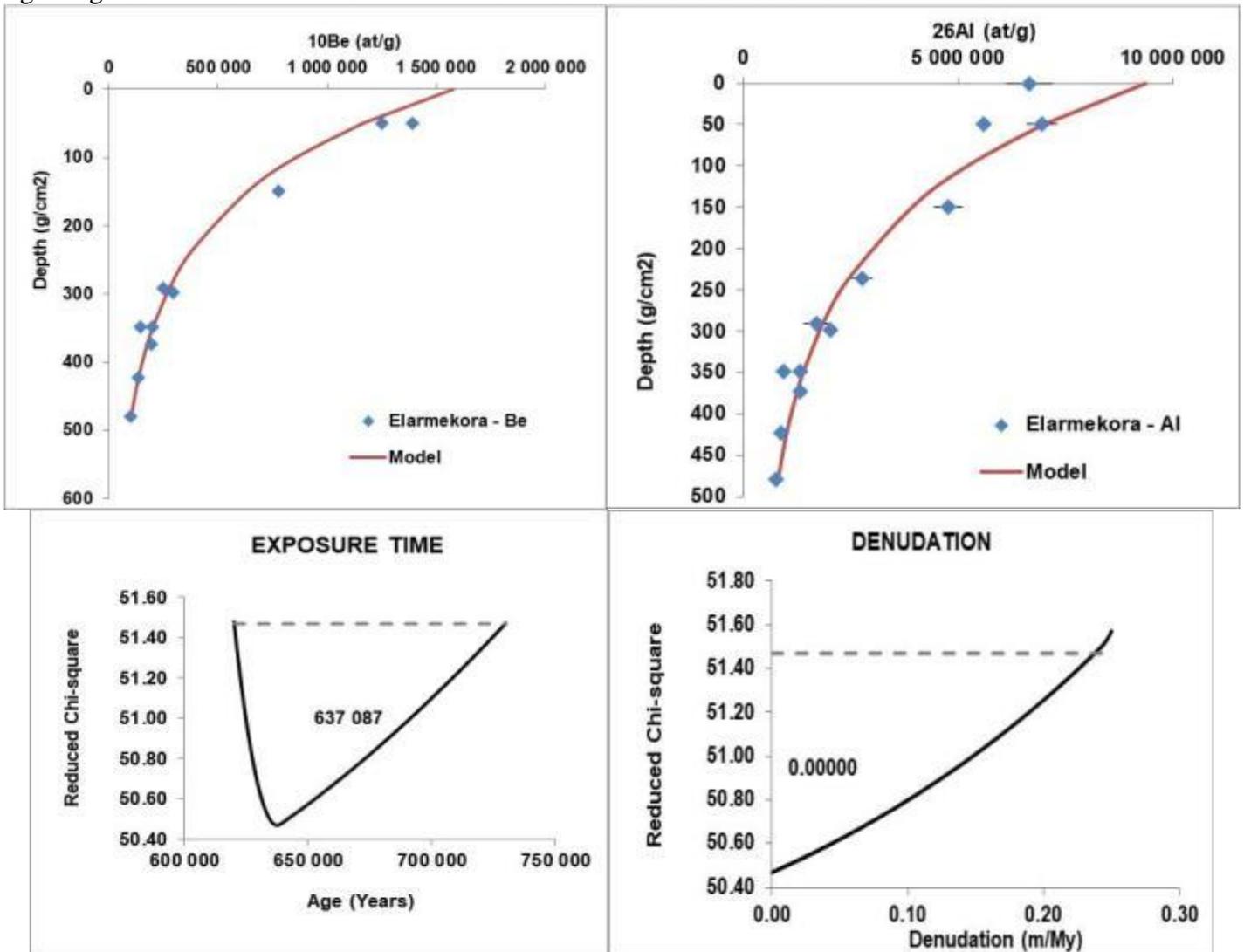
Dash line corresponds to the minimum chi-square plus one equivalent to 1 sigma uncertainty. (Bevington et al. 2003)

3-Model for EKA-TH samples.

Sample	10Be (at/g)	26Al (at/g)
EKA-TH-0	2169.25 ± 40.2	7478.39 ± 225.05

EKA-TH-30	1039.42 ± 21.38	5336.28 ± 176.94
EKA-TH-50	753.51 ± 23.05	4703.95 ± 185.11
EKA-TH-70	605.38 ± 14.46	3415.72 ± 141.21
EKA-TH-90	442.43 ± 13.42	2305.54 ± 89.35

Models outputs for ^{10}Be

```
                        | age (ka) | inheritance (10^4 atoms g^-1) | erosion rate (cm ka^-1) | density (g/ccm) |
|                  mean |  877.051 |                         0.411 |                   0.013 |           2.495 |
|                median |  858.368 |                         0.335 |                   0.011 |           2.496 |
|                  mode |  841.300 |                         0.050 |                   0.010 |           2.499 |
|             min chi^2 |  807.166 |                         0.052 |                   0.003 |           2.500 |
|               maximum | 1179.285 |                         1.494 |                   0.040 |           2.500 |
|               minimum |  772.178 |                         0.000 |                   0.000 |           2.478 |
| Bayesian most probable |  812.121 |                        0.000 |                   0.003 |                 |
| Bayesian 2-sigma upper | 1179.804 |                        1.444 |                   0.042 |                 |
| Bayesian 2-sigma lower |  764.753 |                         NaN |                     NaN |                 |
| Bayesian 1-sigma upper | 1079.952 |                        1.139 |                   0.035 |                 |
| Bayesian 1-sigma lower |  805.623 |                        0.125 |                   0.005 |                 |
```


Models outputs for 26Al

	age (ka)	inheritance (10^4 atoms g^-1)	erosion rate (cm ka^-1)	density (g/ccm)
mean	614.189	15.306	0.043	2.334
median	591.371	13.469	0.042	2.338
mode	502.600	2.630	0.030	2.318
min chi^2	508.166	0.837	0.008	2.249
maximum	988.145	50.604	0.098	2.468
minimum	456.375	0.007	0.000	2.200
Bayesian most probable	506.061	0.000	0.109	
Bayesian 2-sigma upper	1798.588	95.823	0.131	
Bayesian 2-sigma lower	428.570	NaN	NaN	
Bayesian 1-sigma upper	1184.470	55.141	0.111	
Bayesian 1-sigma lower	508.210	2.068	0.023	
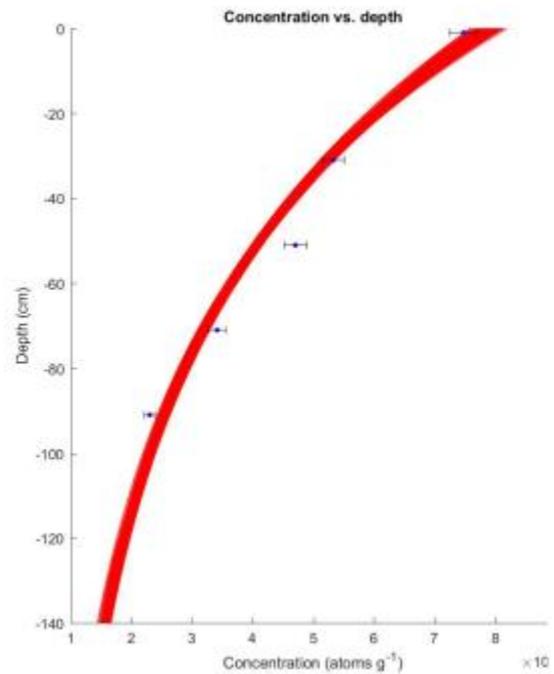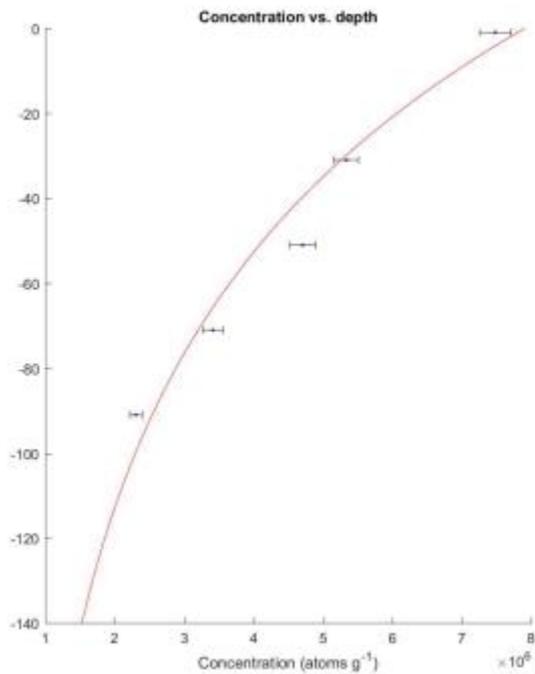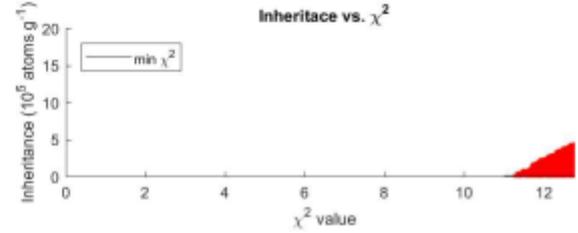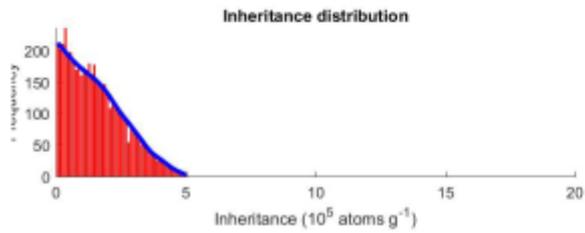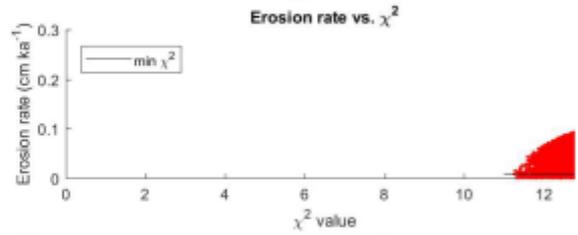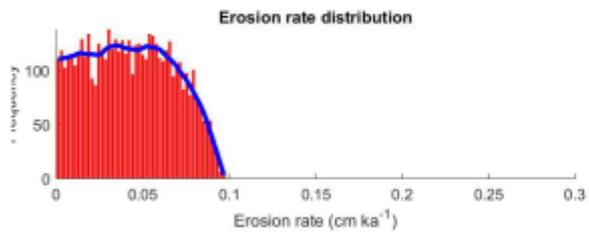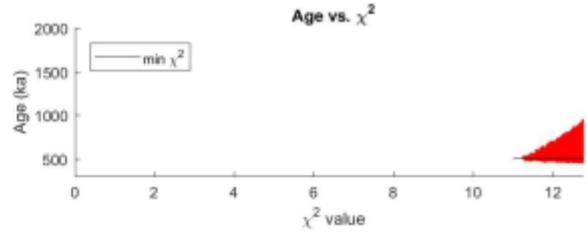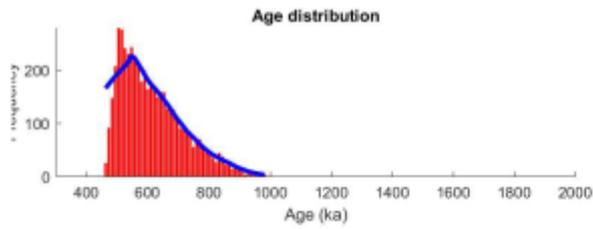
**Model output considering both ^{10}Be and ^{26}Al.**
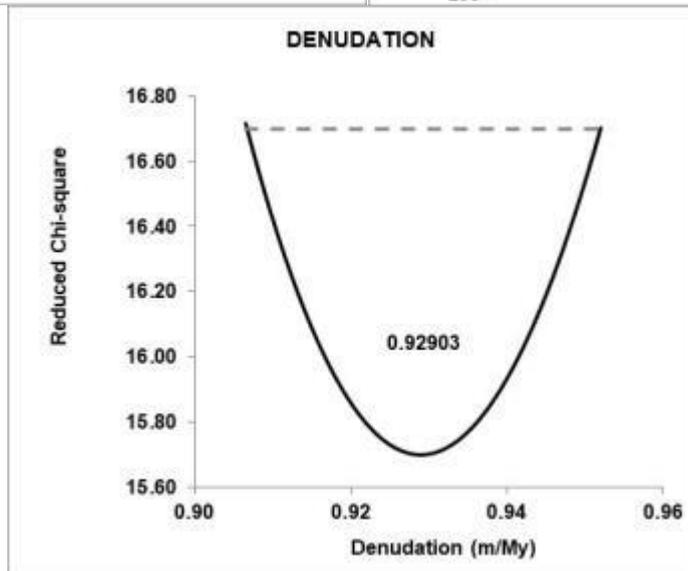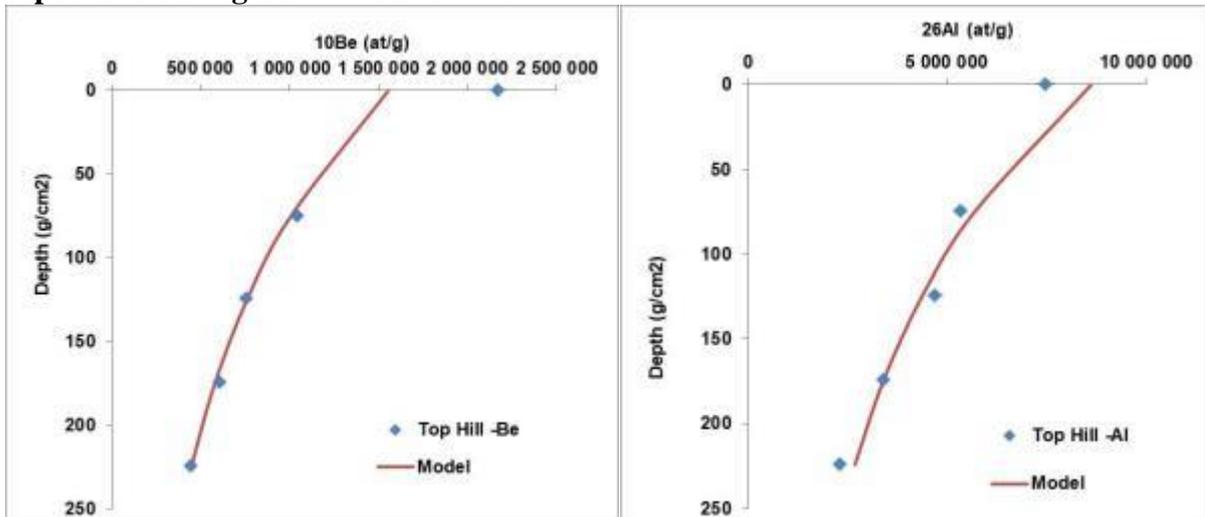
Dash line corresponds to the minimum chi-square plus one equivalent to 1 sigma uncertainty. (Bevington et al. 2003)

4-Composite profile: bottom samples only, those within the saprolite below the alluvial deposit combined with the top hill profile

Sample	10Be (at/g)	26Al (at/g)
EKA-TH-0	2169.25 ± 40.2	7478.39 ± 225.05
EKA-TH-30	1039.42 ± 21.38	5336.28 ± 176.94
EKA-TH-50	753.51 ± 23.05	4703.95 ± 185.11
EKA-TH-70	605.38 ± 14.46	3415.72 ± 141.21
EKA-TH-90	442.43 ± 13.42	2305.54 ± 89.35
EKA19-120	294.7 ± 7.51	2014.51 ± 86.13
EKA19-140	203.09 ± 6.55	1307.49 ± 61.34
EKA19-150	194.96 ± 6	1315.12 ± 62.2
EKA19-170	135.44 ± 4.64	889.12 ± 43.21
EKA19-190-195	100.67 ± 3.26	745.96 ± 73.61

Models outputs for ^{10}Be

```
                        | age (ka) | inheritance (10^4 atoms g^-1) | erosion rate (cm ka^-1) | density (g/ccm) |
                 mean |  877.051 |                         0.411 |                   0.013 |           2.495 |
               median |  858.368 |                         0.335 |                   0.011 |           2.496 |
                 mode |  841.300 |                         0.050 |                   0.010 |           2.499 |
            min chi^2 |  807.166 |                         0.052 |                   0.003 |           2.500 |
              maximum | 1179.285 |                         1.494 |                   0.040 |           2.500 |
              minimum |  772.178 |                         0.000 |                   0.000 |           2.478 |
Bayesian most probable |  812.121 |                         0.000 |                   0.003 |                 |
Bayesian 2-sigma upper | 1179.804 |                         1.444 |                   0.042 |                 |
Bayesian 2-sigma lower |  764.753 |                           NaN |                     NaN |                 |
Bayesian 1-sigma upper | 1079.952 |                         1.139 |                   0.035 |                 |
Bayesian 1-sigma lower |  805.623 |                         0.125 |                   0.005 |                 |
```

Concentration vs. depth

Concentration vs. depth

Models outputs for ^{26}Al

	age (ka)	inheritance (10^4 atoms g^-1)	erosion rate (cm ka^-1)	density (g/ccm)
mean	507.089	0.752	0.003	2.415
median	507.349	0.632	0.002	2.416
mode	507.700	0.060	0.000	2.408
min chi^2	497.692	0.036	0.000	2.390
maximum	528.987	2.847	0.010	2.486
minimum	482.323	0.000	0.000	2.331
Bayesian most probable	509.091	0.000	0.000	
Bayesian 2-sigma upper	588.710	9.634	0.029	
Bayesian 2-sigma lower	443.826	NaN	NaN	
Bayesian 1-sigma upper	548.335	7.673	0.024	
Bayesian 1-sigma lower	474.892	0.885	0.003	
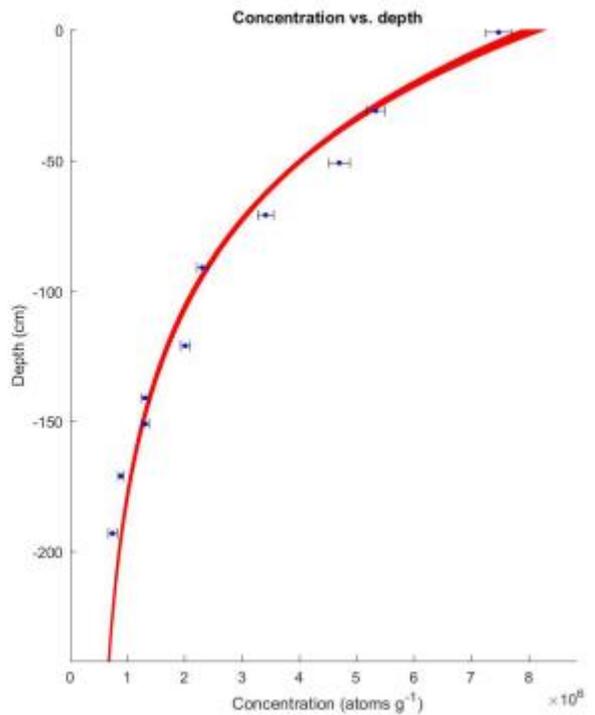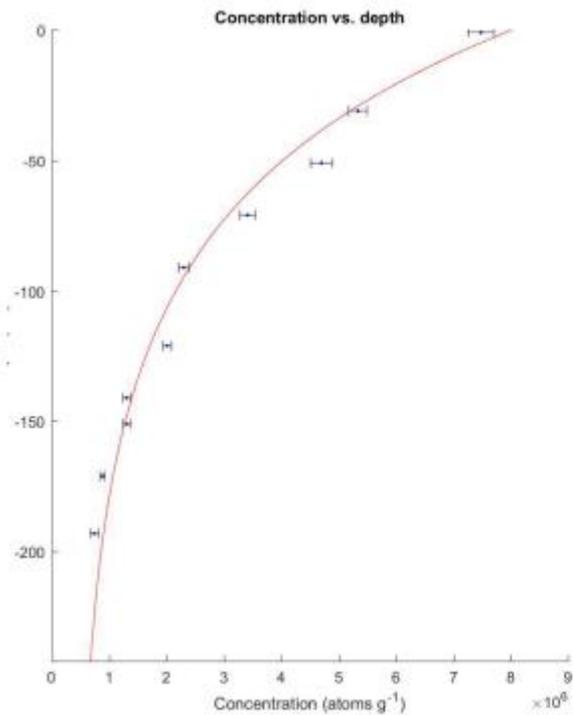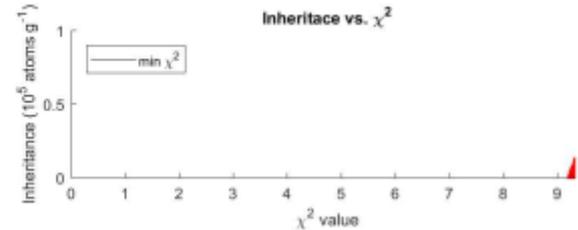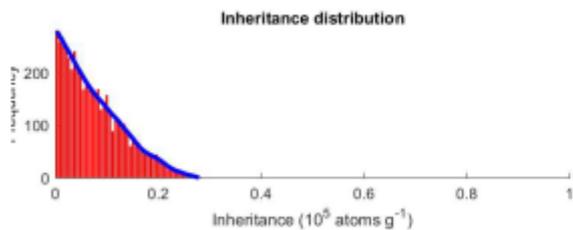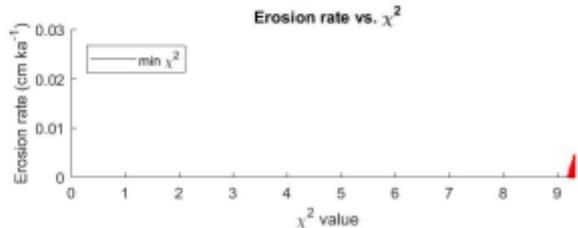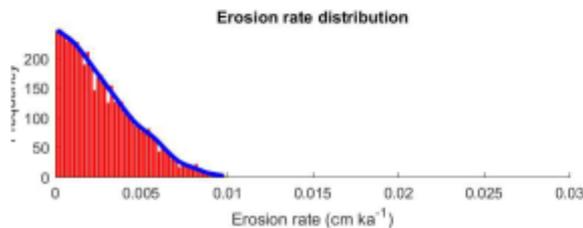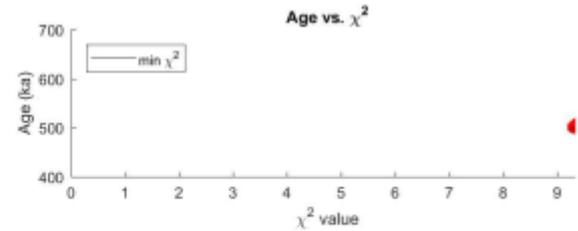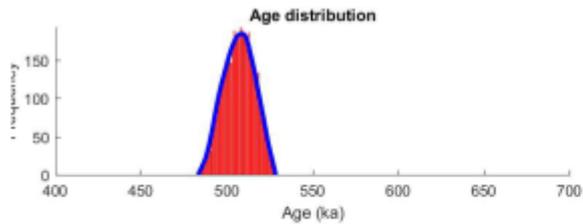
Model output considering both 10Be and 26Al.

Ages range between 700 ka to 1018 ka with a denudation rates range between 0.22and 0.72 m/Ma.
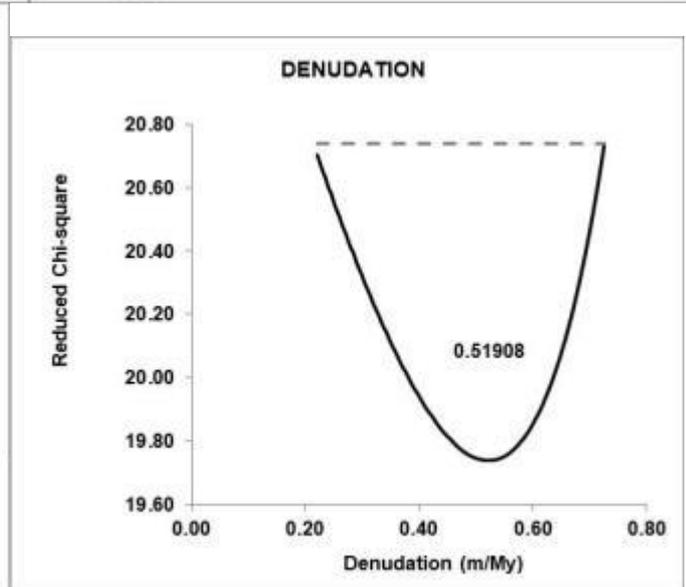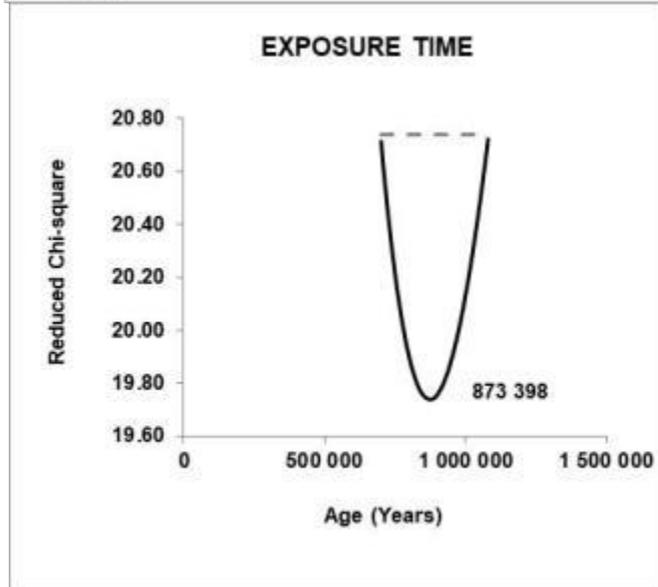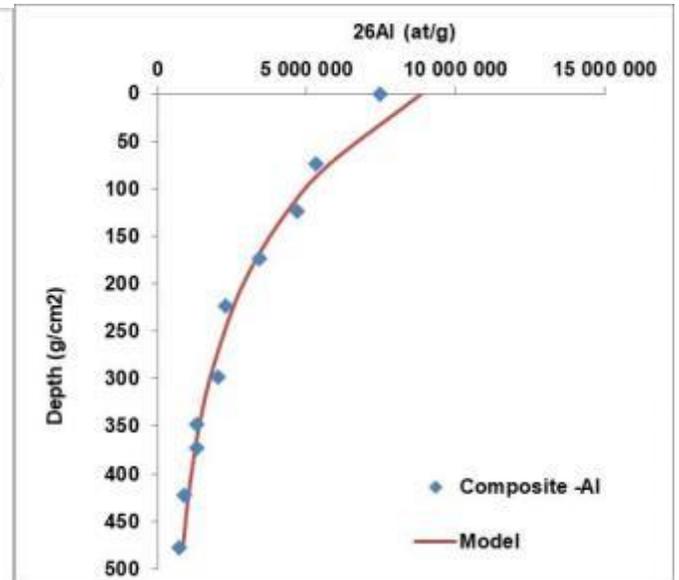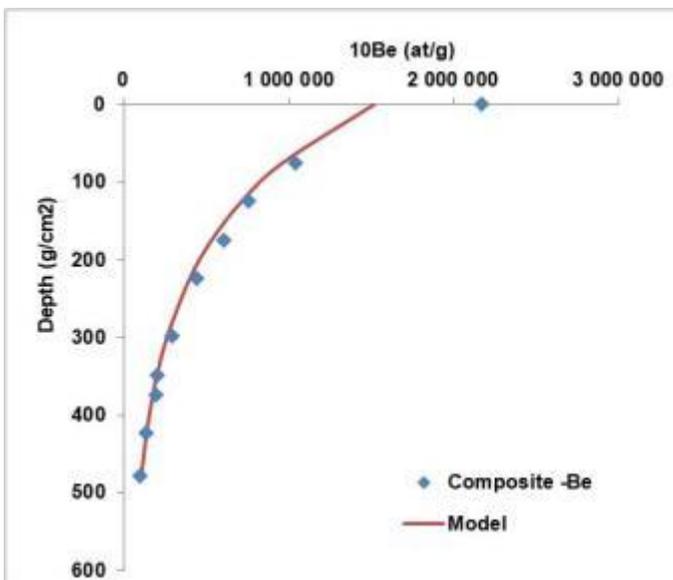
Dash line corresponds to the minimum chi-square plus one equivalent to 1 sigma uncertainty. (Bevington et al. 2003)

References:

Bevington, P.R., and Robinson, D.K., 2003, Data reduction and error analysis for the physical sciences: New York, McGraw-Hill Higher Education, 336 p.

Braucher R, Del Castillo P, Siame L, Hidy AJ, Bourlés DL. In press. Determination of both exposure time and denudation rate from an in situ-produced 10Be depth profile. Quaternary Geochronology 4, 56–67.